Locally real states of photons and particles

Stuart Mirell*
Cyclotron Facility, Building 345, VA GLAHS, 11301 Wilshire Boulevard, Los Angeles, California 90073†
and Department of Radiological Sciences, University of California at Los Angeles, Los Angeles, California 90024
(Received 25 June 2000; revised manuscript received 29 October 2001; published 30 January 2002)

A locally real representation is derived from projections in Hilbert space without arbitrary constants. The inherent enhancement property of the resultant states removes restriction by Bell's theorem. Exact agreement with quantum mechanics is demonstrated by explicit calculations of photon transmission in Malus's law, joint detection probability for correlated photons, spin $\frac{1}{2}$ particle transmission through successive Stern-Gerlach analyzers, and joint detection probability for correlated spin $\frac{1}{2}$ particles. The representation is experimentally testable with respect to quantum mechanics.

DOI: 10.1103/PhysRevA.65.032102 PACS number(s): 03.65.Ta

I. INTRODUCTION

The rapid evolution of the probabilistic interpretation of quantum mechanics from 1925 to 1927 is associated with a departure from the classical principles of realism. In an early attempt to reconcile quantum mechanics and classical principles, de Broglie proposed a reality-based representation at the 1927 Solvay congress [1], but this representation was generally rejected by proponents of the probabilistic interpretation. The tenets of the probabilistic interpretation were crystallized in 1935 by Bohr's response [2] to the analysis of Einstein, Podolsky, and Rosen [3] regarding the question of quantum theory's completeness. Some years later, Bell's theorem [4], based upon apparently plausible assumptions, substantially increased interest in the examination of admissible locally real alternative representations by providing testable criteria. The experimental results of such tests [5] have widely been interpreted as a final validation of the probabilistic interpretation. Despite these events, Popper critically examined the probabilistic interpretation particularly with respect to its philosophical basis [6]. Several researchers, compelled by the firm belief that nonlocality is incongruent with physical reality, have persisted in investigating the boundaries of admissible local alternatives [7–23].

A particular hidden variable model of locally real photon states was presented earlier which demonstrated agreement with the probabilistic interpretation and performed experiments for Malus's law and for correlated photons [24]. The model was shown to be independent of Bell's theorem [4,25] as a consequence of its inherent property of enhancement and was testable. We proceed here from projections in Hilbert space with the derivation of a locally real representation that yields photon states analogous to those of that earlier model. A very closely related self-consistent derivation further extends the representation to include particle states. The resultant comprehensive locally real representation is shown to be in exact agreement with quantum mechanics while providing testable consequences.

States for photons and for particles are deliberately constructed with compatible notation and are presented in substantially self-contained sections in the interests of explicitly elucidating the self-consistency of the respective derivations. As we proceed, we may reasonably anticipate from the calculational success of the quantum mechanical formalism that mathematical analogs may arise in a locally real alternative. Accordingly, any such analogs must be strictly defined as locally real entities and not be imbued with any of the familiar nonlocal probabilistic attributes of quantum mechanics.

A corollary to these concerns is that we must clearly distinguish the locally real representation from Bohm's construction [26]. Bohm basically retains the standard quantum formalism which, together with a potential derived from that formalism, yields a causal interpretation of quantum measurement processes. The Bohm interpretation is appropriately characterized as nonlocally real.

Correlated states and spatially separated superposition states (e.g., two-slit interference [27]) are usually identified as the most notable phenomena that necessitate the imposition of a nonlocal probabilistic interpretation on the underlying standard quantum formalism. These phenomena certainly represent particularly dramatic and self-evident manifestations of nonlocality in the probabilistic interpretation. However, the transmission of photons through successive polarization analyzers (Malus's law) and the passage of particles through successive Stern-Gerlach analyzers are both phenomena well recognized as necessitating the invocation of the probabilistic interpretation given the standard quantum formalism. These phenomena are jointly categorized here as *analyzer emission* processes.

In this regard, we first address these analyzer emission processes from a locally real perspective and then proceed, with benefit of hindsight, to correlated states which turn out to be closely related. Both of these phenomena can be substantially described in the context of single channel analyzers or, equivalently, two-channel analyzers with one blocked channel.

Correspondingly, we defer a detailed locally real alternative to quantum mechanical spatially separated superposition states, which follows directly and consistently from the basis of analyzer emission presented here, but necessitates, in its complete form, the treatment of transmission through two-channel analyzers with both channels open. The physical im-

*Email address: smirell@ucla.edu
†Mailing address.

plications of the locally real representation alternative to these spatially separated superposition states is a subject of some considerable interest and experimental consequences have been examined [28].

The measurement results for photon and particle states considered here are not in any way dependent upon inefficiencies imposed, respectively, on polarization and Stern-Gerlach analyzers (distinct from their associated detectors). Accordingly, we are free to treat these analyzers as idealized.

The phenomena we examine here, when represented quantum mechanically, particularly characterize the tenets of the probabilistic interpretation. We will abide by the general convention in which that probabilistic interpretation is implied when using the term quantum mechanics.

II. LOCALLY REAL PHOTON STATES

A. Introduction to photon states

Following the example of quantum field theory, we treat the vacuum field as a collection of harmonic oscillators in random ground state motion. The functional specification $\Phi(z,t;b_\gamma)$ that we utilize here for a photon propagating along the z axis is substantially equivalent to the wave function of the usual quantum formalism but represents in the present context a wave structure consisting of a subset of the (real) oscillators in coherent motion orthogonal to z. The passage of Φ through a local region is effectively a coherence wave that drives resident random ground state oscillators into transitory coherent (ground state) motion. A superposition of constituent harmonic waves with a dispersion of wave numbers k_n gives Φ its functional amplitude with respect to the propagation axis as shown in Fig. 1(a). The parameter b_γ is a coefficient that scales this amplitude. The evaluation of $\Phi^*\Phi$ provides a proportionate measure of the density of oscillators in coherent ground state motion orthogonal to the propagation axis as a function of z,t. Since Φ is not a probabilistic entity, there is no inherent requirement to normalize $\Phi^*\Phi$.

For a specific photon emitted at $t=0$ and propagating along the z axis, the temporal and spatial evolution of Φ is substantially equivalent to that of the quantum mechanical formalism with the explicit understanding that the wave structure is a real entity.

Φ, defined on $t\geqslant 0$, is clearly descriptive of a dominant aspect of the photon's structure; however, the parameters z, t, and b_γ provide no information regarding ''polarization'' properties. For a specific photon, this information is contained in the variables Δ_γ and θ_γ defined in the plane orthogonal to the propagation axis. The quantities Δ_γ and θ_γ as well as b_γ are identifiable as ''hidden variables.'' However, we shall apply the term *field variables* instead, as more appropriate in the full objective context of the locally real representation.

We will necessarily have frequent occasion to assume this objective perspective in which the field variables Δ_γ, θ_γ, and b_γ of a given photon are specified. This perspective is permissible in a representation of real entities even though subjectively (experimentally) we cannot have complete knowledge of the particular field variable values for any given photon.

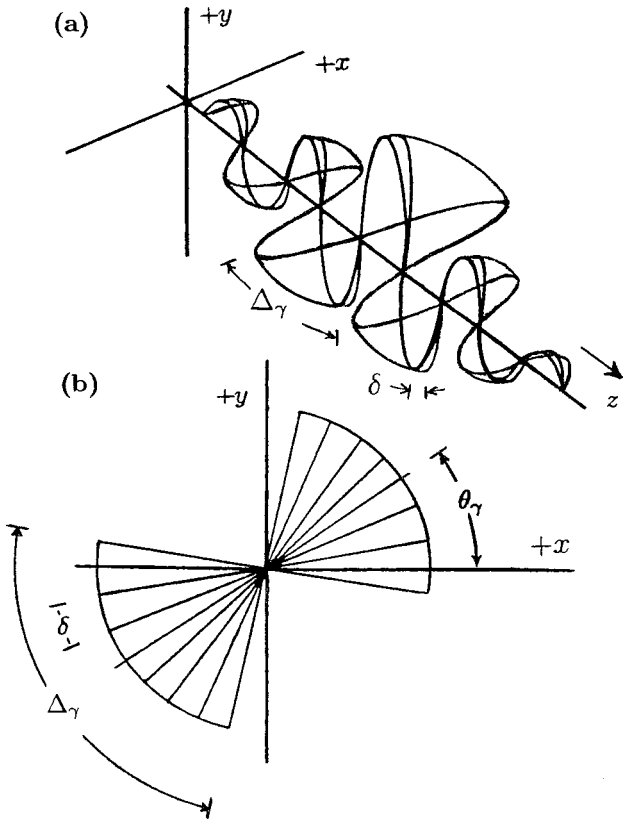

FIG. 1. Photon wave structure (a) represented by the associated wave function amplitude along the z propagation axis rotated through an arc Δ_γ. The entire structure is scaled by an amplitude coefficient b_γ. A constituent planar wave packet of infinitesimal arc δ is shown near the plane of the y axis. Schematic representation of a photon's collective planar wave packets (b) viewed projectively along the propagation axis, shows total arc span Δ_γ and orientation of the photon (arc span bisector) θ_γ. Intersection of depicted Δ_γ arc with an analyzer's polarization axis, e.g., along the x axis, results in photon's transmission.

Objectively, the wave function of a specific photon is then more completely specified as $\Phi(z,t;\Delta_\gamma,\theta_\gamma,b_\gamma)$. In this regard we define a *planar wave packet* as a subgroup of coherent Φ oscillators moving orthogonal to the propagation axis in an infinitesimal angular arc δ oriented at some particular angle about that axis as represented in Fig. 1(a).

A given photon consists of a set of these planar wave packets, all with a uniform amplitude coefficient b_γ. The packets are contiguously arrayed about the propagation axis and collectively subtend a finite angular arc Δ_γ as shown in Fig. 1(a) and, schematically as a projective axial view, in Fig. 1(b). The magnitude of Δ_γ ($=N\delta$ for some integer N) and the orientation of the Δ_γ bisector at some θ_γ are essential field variables characterizing a particular photon. An orientation at θ_γ is equivalent to $\theta_\gamma+\pi$ because of the bidirectionality of the planar packets. The two opposed arcs in Fig. 1(b) are then appreciated as representing the same set of planar packets but with a relative π phase shift along the propagation axis. In the consideration here of photon states

and their measurement, it is convenient to treat the δ of each planar packet as a suitably small but finite angular increment. Ultimately, as the limit $\delta \to 0$ is applied while $N \to \infty$, $\Delta_\gamma = N\delta$ remains constant and we see that the discrete planar packet is purely a mathematical intermediary.

The general physical characteristics of Φ emerging from this construction are that all photons generated under experimentally equivalent conditions have substantially identical wave structures (to within an amplitude scale factor of b_γ) with respect to z and t dependence but differ in the fixed values of Δ_γ, θ_γ, and b_γ associated with the angularly arrayed wave packets of a particular photon.

We shall shortly demonstrate the relationship of the Δ_γ, θ_γ, and b_γ field variables to the ''polarization'' of the photon and to analyzer measurement of that polarization. However, the primary task at hand is the derivation of the underlying formalism that assigns particular field variable values to emitted photons. This formalism generates a wave function associated with an ensemble of photons defined at the emission source at $t<0$. The allowable Δ_γ and θ_γ values, in their proper frequency distribution, map to the members of this ensemble. As a stochastic process, a random member of the ensemble is emitted at $t=0$ with particular objectively fixed values Δ_γ and θ_γ giving an associated wave function $\Phi(z,t;\Delta_\gamma,\theta_\gamma,b_\gamma)$ for $t \geqslant 0$. We shall see that any specific emitted ensemble member is a real definable physical entity with an objectively deterministic transmission outcome through some distant polarization analyzer.

The energy quantum associated with a photon exists as an excitation state on one of the constituent coherent ground state oscillators. The excitation migrates on Φ with an instantaneous probability along the propagation axis proportionate to $\Phi^*\Phi$. The excitation also migrates on the contiguous set of wave packets with a random instantaneous probability on any individual packet of the angular arc Δ_γ.

The probabilities associated with the excitation locus on the photon's wave structure are readily shown to be independent of the amplitude coefficient b_γ. The probability independence on the set of the Δ_γ arc of packets is immediately seen from the uniformity of b_γ on those packets. The probability independence along the propagation axis can be appreciated by observing that the density of coherent oscillators given by $\Phi^*\Phi$ is scaled by the particular value of b_γ^2 for that photon. However, this scaling does not alter the relative likelihood of the excitation being at a particular z,t on a single spatially contiguous wave structure.

Conversely, for processes such as the intersection of spatially separated wave structures, the relative value of b_γ on each structure is critical to excitation dynamics in the resultant wave interference. Nevertheless, because we confine our present considerations almost entirely to phenomena involving single channel analyzers, such spatially separated wave structures do not arise and the specification of b_γ is largely superfluous in that regard. Most significantly in the context of the present paper, we will demonstrate that a photon's transmission outcome through an analyzer is also independent of b_γ. Accordingly, we will explicitly consider the amplitude coefficient b_γ only when its inclusion contributes to a more complete understanding of the locally real structure. Otherwise, the particular value of b_γ can, in principle, be suppressed here in our specifications of field variables.

In the locally real representation, it is the excitation that provides us with a probe of the photon wave packet structure of Φ with particular regard here to z,t dependence. Various measurement procedures applied to individual photons can reveal the instantaneous value of a parameter such as position z or wave number k_n associated with the excitation as it moves on the wave packet structure. Ultimately, after conducting a large number of such measurements on similarly emitted photons, a map of $\Phi^*\Phi$ along the propagation axis can be ascertained. The $\Delta z, \Delta k_n$ uncertainty on a real field is seen as a manifestation of the classical relationship of canonically conjugate variables such as z,k_n in the construction of a wave packet for which $\Delta z \Delta k_n \approx 2\pi$.

B. Analyzer emission of photons

From the perspective of local reality, the statistical distribution of photon transmission outcomes through some distant analyzer A' must originate at the emitting analyzer A. We postulate that any particular photon emitted by analyzer A is a random member of an ensemble of photons and seek a mathematical representation of this ensemble consistent with the physically known properties of photon transmission through polarization analyzers.

The ensemble necessarily arises from a photon propagating within the analyzer. We designate this photon as a *generator photon* γ_g. For a trial solution we then consider an *analyzer emission ensemble* derived from projections in the transverse plane specifically originating at the polarization axis as γ_g reaches the analyzer's exit face. This solution implies that the γ_g wave structure is narrowly confined to the plane of the analyzer's polarization axis within some angular arc δ as it propagates within the analyzer. Because of this physical confinement, γ_g is characterized as being in *δ-form*. We proceed with this physical representation of γ_g as we construct the analyzer emission ensemble and subsequently reexamine this representation for self-consistency.

The analyzer emission ensemble that we construct constitutes the objective specifications of a representative set of photons potentially emitted by an analyzer. We assign a set of $|u_k\rangle$ orthonormal basis vectors in Hilbert space in one to one correspondence with the angular coordinate $\theta = k\delta$ for integer values of k where $|k\delta| \leqslant \pi/2$. We ultimately obtain an infinite dimensional Hilbert space as $\delta \to 0$. The analyzer's polarization axis is chosen to coincide with the x axis where $\theta = 0$ in real space.

When an internally propagating δ-form generator photon γ_g, associated with the basis vector $|u_0\rangle$, reaches the exit face of the analyzer, a set of projected packet state vectors

$$|\phi_k\rangle = \cos(k\delta)|u_k\rangle \tag{1}$$

is generated. This set is used to construct the analyzer emission ensemble.

The ensemble's *analyzer emission superposition state*

$$|\phi_e\rangle = \sum_{j=m}^{n} |\phi_j\rangle = \sum_{j=m}^{n} \cos(j\delta)|u_j\rangle \tag{2}$$

is constructed from the Eq. (1) state vectors where $n = \pi/(2\delta) = -m$. Analyzer emission superposition states associated with arbitrary polarization analyzers are all identical to Eq. (2) after translating to a frame in which $|u_0\rangle$ is associated with the γ_g propagating in the plane of the emitting analyzer's polarization axis. The generator photon γ_g orientation and the ensemble's ''centroid'' orientation are then both given by $|u_0\rangle$ in Hilbert space.

For analyzer emission ensembles, each constituent $|\phi_k\rangle$ Eq. (1) packet state vector is a single state formed with the corresponding $|u_k\rangle$ basis vector because the projections originate from a single basis vector. As a consequence, each $|\phi_k\rangle$ packet state vector is identified as the projection of the ensemble's analyzer emission superposition state $|\phi_e\rangle$ into the $|u_k\rangle$ Hilbert subspace. In the present context, this property is of a trivial nature. However, it will be instructive to examine the analogous projections when we consider correlated photons.

The norm of $|\phi_k\rangle$ is

$$\|\phi_k\| = \langle \phi_k|\phi_k\rangle^{1/2} = \cos(k\delta), \tag{3}$$

which is equivalent to the amplitude of a particular projected state vector $|\phi_k\rangle$,

$$\langle u_k|\phi_k\rangle = \cos(k\delta), \tag{4}$$

as well as the amplitude of the analyzer emission superposition state at some $|u_k\rangle$,

$$\langle u_k|\phi_e\rangle = \cos(k\delta). \tag{5}$$

Physically, each of these quantities may be viewed as a $\cos(k\delta)$ projection from the $k\delta$-distant generator photon.

Squaring either amplitude gives the probability of an ensemble planar packet at a particular $|u_k\rangle$:

$$\langle u_k|\phi_k\rangle^2 = \langle u_k|\phi_e\rangle^2 = \cos^2(k\delta). \tag{6}$$

The functional cosine squared probability of ensemble planar packets specified in Eq. (6) is depicted in Fig. 2. From this probability we now seek the compilation of these planar packets into an ensemble set of emission photons.

In the interests of determining this compilation, we consider the requisite criteria for transmission of a photon through an analyzer. The photon we select is a particular ensemble member of an emission analyzer A. That photon, when incident on some distant analyzer A', must first propagate within that analyzer as a δ-form generator photon γ_g' before being transmitted as an emission ensemble member of A'. The accompaniment of the excitation in this process is an implicit requirement if the resultant emitted A' ensemble member is to be defined as a (potentially detectable) transmitted photon.

We postulate that an excitation migrating on the photon's wave structure has physical accessibility to any particular wave packet on some collective arc Δ_γ because of the contiguity of those packets. Consistent with this property, the excitation also has physical accessibility to the δ-form wave structure arising within the analyzer only when the Δ_γ of an incident photon intersects the analyzer's polarization axis. Since photons emitted from an analyzer are known to have a 0.5 probability of transmission through a subsequent, randomly oriented, analyzer, we anticipate that emission ensemble members are characterized by a contiguous $\Delta_\gamma = \pi/2$ arc of packets which yields that 0.5 probability. We define $\Delta_\gamma = \pi/2$ photons as having a *full complement* of packets.

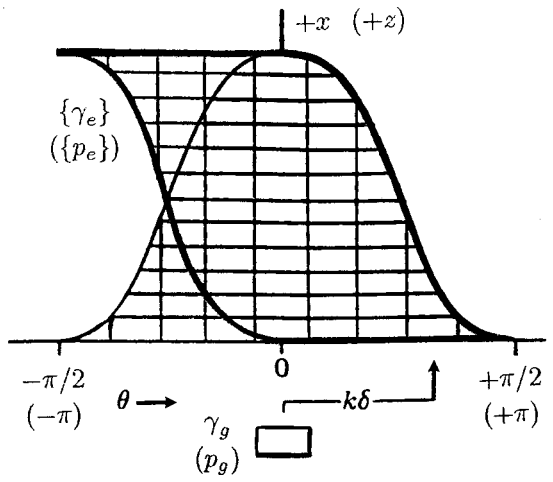

FIG. 2. The $\cos^2\theta$ function gives the angular probability of planar wave packets emitted from a polarization analyzer and associated with an internally transmitted photon γ_g with packets condensed along the analyzer's polarization axis at $\theta = 0$. The angular probability is unaltered by inversion of the $\cos^2\theta$ contour for $\theta < 0$. A photon γ_e emitted by the analyzer is a random member (row) of the ensemble $\{\gamma_e\}$ defined by the modified (bold) contour. Alternatively, for particles, substituting the quantities in parentheses gives a $\cos^2(\theta/2)$ contour representing the angular probability of spin wave packets emitted from a Stern-Gerlach analyzer and associated with an internally transmitted particle p_g with packets condensed along the analyzer's magnetic axis at $\theta = 0$. Similarly, a $\theta < 0$ inversion gives a modified contour defining the ensemble $\{p_e\}$. A particle p_e emitted by the analyzer is a random member (row) of $\{p_e\}$.

The compilation of the emission packets into an ensemble of photon members is then particularly straightforward given the above considerations. An inspection of the Fig. 2 $\cos^2\theta$ wave packet probability yields the requisite solution by noting that the probability as a function of θ is invariant under an inversion of the $\theta < 0$ packet contour to $1 - \cos^2\theta$. In the modified form of the contour we identify the set of photons defined by the rows of wave packets. This set of full complement photons uniquely constitutes the requisite ensemble $\{\gamma_e\}$. Any single γ_e emitted as a stochastic process from an analyzer A is a random member (row) of the associated ensemble. Each member has a contiguous arc of packets $\Delta_\gamma = \pi/2$. Summed over multiple emitted photons, the ensemble and the $\cos^2\theta$ wave packet probability are trivially recovered.

An ensemble's wave packet probability specified by Eq. (6) and depicted in the modified Fig. 2 contour may also be

regarded as the ensemble's wave packet distribution. There is an effective equivalence of these two terms in the treatment of photon ensembles since both quantities are represented in their entirety in the plane orthogonal to the propagation axis. (However, in our treatment of particles we will encounter an exception to this equivalence arising from the three-dimensionality of relevant distributions.)

We can now consider the ensemble members emitted from an analyzer A interacting with a second polarization analyzer A' rotated by $\theta = k\delta$ with respect to A. We see that a $\cos^2\theta$ fraction of the ensemble members have a Δ_γ that intersects θ, resulting in transmission, which gives us agreement with Malus's law for the representation. Note that the representation is explicitly locally real. The state of a photon incident on analyzer A' is in no way altered by the physical orientation of that analyzer. Photons are not regarded as binary quantum objects with a horizontal or vertical polarization. From the ensemble construction, the members of $\{\gamma_e\}$ have a continuum of orientations given by the bisector angles θ_γ of the rows in the modified contour of Fig. 2. Furthermore, the transmission outcome for a random member incident on A' is fully deterministic the instant that particular member leaves analyzer A with an objectively defined packet arc Δ_γ with orientation θ_γ. For that photon to be transmitted by A', its packet arc Δ_γ must intersect the A' polarization axis. The photon's emergence from A' is then as a member of a new ensemble generated from $|u_0'\rangle$ associated with the A' polarization axis at $\theta' = 0$. Consequently, we have transmission consistent with Malus's law for any number of arbitrarily rotated sequential analyzers.

It is instructive at this point to examine the underlying differences between the locally real representation and quantum mechanics. For this examination, we again consider photons transmitted through an analyzer A with its polarization axis oriented at $\theta = 0$ along the x axis and a subsequent analyzer A' rotated at some θ.

The strict probabilistic interpretation of quantum mechanics requires that the photon transmitted through analyzer A be in a definite state $|\phi_{qm}\rangle = |x\rangle$ where $|x\rangle$ and $|y\rangle$ are orthonormal basis vectors in a two-dimensional Hilbert space. In this interpretation, the role of the measurement process is central to the assignment of states. That photon, when measured by a subsequent analyzer A' rotated by θ, must now be in a binary superposition state

$$|\phi_{qm}\rangle = (\cos\theta)|x'\rangle + (\sin\theta)|y'\rangle \tag{7}$$

by a projective transformation to the new basis pair $|x'\rangle$ and $|y'\rangle$ of A'. The respective amplitudes of the photon being in the states $|x'\rangle, |y'\rangle$ are

$$\langle x'|\phi_{qm}\rangle = \cos\theta, \quad \langle y'|\phi_{qm}\rangle = \sin\theta \tag{8}$$

with corresponding probabilities

$$\langle x'|\phi_{qm}\rangle^2 = \cos^2\theta, \quad \langle y'|\phi_{qm}\rangle^2 = \sin^2\theta \tag{9}$$

for the inherently binary measurement outcomes.

Quantum mechanics requires that the assignable states be a binary superposition prior to measurement, and, after measurement, the collapse of one of the states places the photon in a single definite state of the other. The requisite Hilbert space is two dimensional. Because of the role of the measurement process in assigning photon states, the photon itself is necessarily treated as a probabilistic entity. Moreover, all photons emitted from an analyzer are identical probabilistic entities. They are distinguishable only upon measurement as a purely probabilistic consequence of assuming one of the two possible states of the superposition. Quantum mechanics regards these probabilistic entities as nonreal.

In the locally real representation, the transverse state of a particular photon γ emitted by an analyzer can be objectively specified by the superposition state

$$|\Phi_\gamma\rangle = \sum_{j=m}^{n} |u_j\rangle \tag{10}$$

defined on a Hilbert space (which becomes infinite as $\delta \to 0$) with orthonormal $|u_j\rangle$ basis vectors. Here $\Delta_\gamma = \pi/2 = (n-m+1)\delta$ and $\theta_\gamma = \frac{1}{2}(n+m)\delta$. Equation (10) explicitly requires that the photon be "in" all of the $|u_j\rangle$ states associated with the packet arc Δ_γ at θ_γ. This property is demonstrated by the probability $\langle u_k|\Phi_\gamma\rangle^2 = 1$ for all $|u_k\rangle$ associated with Δ_γ. Each of these occupied states represents an objectively real planar wave packet.

In the locally real representation, any analyzer A', positioned subsequent to an emission analyzer A, has no role in the Eq. (10) specification of an emitted photon's superposition of states. Objectively, the infinite $|u_j\rangle$ states associated with Δ_γ exist independently of any measurement device.

If the subsequent analyzer A' has its polarization axis at some θ associated with a particular $|u_k\rangle$ in the Hilbert space of the emission analyzer, a transmission outcome experimentally establishes only that $|u_k\rangle$ was one of the constituent states of the incident photon $|\Phi_\gamma\rangle$ and an absorption outcome establishes the converse. Objectively, the outcome is deterministically fixed the instant the photon is emitted from A and the constituent states of $|\Phi_\gamma\rangle$ are specified.

Experimentally, however, we have knowledge only that any photon emitted by A is a member of an ensemble constructed from the Eq. (2) analyzer emission superposition state $|\phi_e\rangle$. We can then examine this ensemble using a subsequent analyzer A' rotated by $\theta = k\delta$ which associates A' with some basis vector $|u_k\rangle$. The probability of a random ensemble member emitted by A having a constituent state $|u_k\rangle$, i.e., a planar wave packet associated with that state, was shown in Eq. (6) to be $\cos^2(k\delta)$. Since those members having a state at $|u_k\rangle$ are transmitted, we showed that $\cos^2(k\delta)$ is equivalently also the probability of transmitting a random ensemble member and, consequently, gives us Malus's law.

This result can be made even more explicit by noting that an ensemble member is successfully transmitted through a subsequent analyzer A' only when it transitionally assumes the form of a generator photon as it enters that analyzer. In the Hilbert space of A', the state of this generator photon $|\Phi_g'\rangle = |u_0'\rangle$ since the generator photon is, by construction, in the single state associated with the A' polarization axis. A rotational translation between the Hilbert spaces of the re-

spective analyzers implies that in the frame of A there is a $|u_k\rangle = |u_0'\rangle$, resulting in a modified form of Eq. (6):

$$\langle \Phi_g' | \phi_e \rangle^2 = \cos^2(k\delta). \tag{11}$$

The particular expression of Malus's law given by Eq. (11) is suggestive of a quantum mechanical transition probability $|\phi_e\rangle \rightarrow |\Phi_g'\rangle$ at A'. However, from the objective perspective of local reality, this interpretation is misleading because $|\phi_e\rangle$ is not a single definite state at $|u_0\rangle$ as in quantum mechanics, but represents an ensemble of packet states with centroid at the basis vector $|u_0\rangle$ and a distribution defined over the infinite set of $|u_j\rangle$ basis vectors. In the infinite dimensional Hilbert space of the locally real representation, the ensemble is effectively a superposition of wave packet states that, as a stochastic process, emits a random member at A that is itself a superposition of wave packet states. Most importantly, we must be clear that $|\phi_e\rangle$ is not present at A' since it ceased to exist the instant the ensemble member left A.

The physical significance of a particular photon's superposition state Eq. (10) can further be understood by the evaluation of

$$\langle \Phi_\gamma | \Phi_\gamma \rangle = N = \pi/(2\delta). \tag{12}$$

Equation (12) gives the sum of the Eq. (10) particle's packet probabilities over a full π angular span of the $2N$ Hilbert space basis vectors $|u_j\rangle$. The N individual unit probability terms associated with a particular objectively specified photon confirm that N packets are present on that angular span. Equation (12) simply reminds us once again that in the locally real representation a photon with N packets is ''in'' all of the states occupied by these objectively real packets. Accordingly, our sum over probabilities is appropriately N and not unity. Objectively, the inherent multiplicity of packet states in the locally real representation explicitly necessitates the use of a corresponding multidimensional Hilbert space, which goes to infinity as $\delta \rightarrow 0$, in contrast to measurement-based quantum mechanics which requires a two-dimensional Hilbert space as a consequence of the binary observable outcomes. Of course, when we reach the limit $\delta \rightarrow 0$, the state of the photon is objectively described by Δ_γ and θ_γ. The formalism of a multidimensional Hilbert space is seen as a mathematical intermediary.

After a photon is emitted, we can examine additional properties by representing that objectively realized photon in Euclidean space. This representation, while not applicable to the construction of the emission ensemble, provides a powerful tool for gaining physical insight into the structure of such realized photons. In particular, the representation in Euclidean space allows us to understand the role of the amplitude coefficient b_γ. For these purposes, we select a reference frame with the z axis oriented along photon trajectories and the x axis aligned with the polarization axis of an analyzer A.

We first consider a particular incident photon such as the example in Fig. 1(b) with an arc $\Delta_{\gamma i} = \pi/2$, an orientation $\theta_{\gamma i}$ from the analyzer's polarization axis, and a uniform packet amplitude coefficient $b_{\gamma i}$. We can make these specifications for an objectively real photon and examine the measurement consequences even though we have no experimental means of selectively generating any particular photon at will. The set of packets of this physically realized photon can be represented in the two-dimensional Euclidean space orthogonal to the propagation axis by an equivalence set of $b_{\gamma i}$ magnitude radial vectors each oriented at the respective angle of its packet, giving

$$\mathbf{\Phi}_{\gamma i} = b_{\gamma i} \sum_{j=m}^{n} \hat{\mathbf{r}}_j, \tag{13}$$

where $(n-m+1)\delta = \Delta_{\gamma i} = \pi/2$, $(n+m)\delta/2 = \theta_{\gamma i}$, and the $\hat{\mathbf{r}}_j$ are unit radial vectors oriented at the $\theta = j\delta$ of the respective packets. Equation (13) should be compared to the corresponding Eq. (10) representation of a photon in Hilbert space. Both equations relate only to the transverse aspect of a photon's wave structure.

In Euclidean space we begin with the Eq. (13) representation of an objectively real set of packets and examine the role of the amplitude coefficient as a photon enters and exits an analyzer.

With respect to the example in Fig. 1(b), the present analysis of a particular photon is applied to the $\pi/2$ arc of packets on the right. The left arc, which merely provides mirror redundancy, represents the same packets phase shifted along the propagation axis by π.

When the photon begins to enter analyzer A, the vector amplitude $b_{\gamma i}$ of each individual packet rapidly reduces to zero and, simultaneously, projects its component along the polarization axis onto that axis (chosen here as the x axis). Collectively, the vector sum of these projected packet vector components results in a ''superpacket'' of amplitude coefficient b_δ ($\gg b_{\gamma i}$) ''condensed'' along the polarization axis of the analyzer in δ-form.

Alternatively, this superpacket amplitude b_δ can readily be computed by first forming the vector sum of the incident photon packet vectors, which yields a resultant vector oriented at $\theta_{\gamma i}$ [$= \theta_\gamma$ in Fig. 1(b)]. The magnitude $M_{\gamma i}$ of this resultant vector can be determined by integrating the projective components with respect to the bisector of an arbitrary $\Delta_\gamma = \pi/2$ arc. Integration of the discrete packet contributions is valid as $\delta \rightarrow 0$. The magnitude of the resultant vector is

$$M_{\gamma i} = \frac{b_{\gamma i} \int_{-\pi/4}^{\pi/4} (\cos\theta) d\theta}{\delta} = \frac{\sqrt{2} b_{\gamma i}}{\delta}. \tag{14}$$

Then the resultant vector's component projected onto the polarization axis has an amplitude coefficient

$$b_\delta = \frac{\sqrt{2} b_{\gamma i} \cos\theta_{\gamma i}}{\delta}. \tag{15}$$

The ''single'' superpacket photon

$$\mathbf{\Phi}_\delta = b_\delta \hat{\mathbf{x}} \tag{16}$$

propagates through the analyzer, condensed along the analyzer's polarization axis defined here as the x axis. $\mathbf{\Phi}_\delta$ is clearly a Euclidean space representation of a generator photon γ_g. As we impose the mathematical limit $\delta \rightarrow 0$, the number N of planar wave packets that are associated with an incident photon's finite Δ_γ goes to infinity. Consequently, with N individual $b_{\gamma i}$ amplitudes contributing their respective components along the analyzer's polarization axis, the vector sum of the resultant superpacket has an amplitude coefficient $b_\delta \rightarrow \infty$ as demonstrated by Eq. (15). However, the integral of $\mathbf{\Phi}_\delta$ over the angular δ of the superpacket at the polarization axis,

$$\int_\delta \mathbf{\Phi}_\delta d\theta = b_\delta \int_\delta d\theta\, \mathbf{x} = \sqrt{2} b_{\gamma i} (\cos \theta_{\gamma i}) \mathbf{x}, \tag{17}$$

remains finite giving the δ-form superpacket photon $\mathbf{\Phi}_\delta$ a formal equivalence to a Dirac δ function.

Classical electromagnetics provides a compelling physical rationale for this condensation process along the polarization axis. This rationale is appropriately considered in the context of a multiplicity of photons on a plane polarized beam. The multiplicity of realized photons can be represented by the members of an emission ensemble. The critical property of the ensemble in this regard is the symmetrical distribution of its member's (arc bisector) orientations θ_γ about the centroid orientation that coincides with the polarization axis of an emitting analyzer. We can then identify the orientation of a plane polarized beam with that of the ensemble's centroid. It is therefore meaningful to specify the ''polarization'' of an ensemble. Subjectively, it is also appropriate to attribute this ''polarization'' to all individual photons associated with a particular ensemble. Consequently, an individual photon, which subjectively has the property of ''polarization,'' objectively may be further specified as having a definite orientation at some particular θ_γ.

The familiar type of polarization analyzer we consider here consists of a transmissive dielectric plate with an atomic structure exhibiting parallel linear conduction paths. The polarization axis lies orthogonal to these conduction paths in the plane of the analyzer.

At the level of classical electromagnetics, we examine a plane polarized beam of photons, characterized by some electric vector **E**, incident on an analyzer with its polarization axis along some unit vector $\hat{\mathbf{r}}_\theta$ rotated by θ from **E**. We know that the component of **E** along the conductive paths is strongly absorbed as the beam enters the analyzer. Consequently, the remaining beam propagating within the analyzer is characterized by the component of **E** projected identically along the polarization axis, $\mathbf{E} \cdot \hat{\mathbf{r}}_\theta \hat{\mathbf{r}}_\theta$.

We hypothesize that there is a direct physical correspondence between the electromagnetic wave and the wave structure in the locally real representation. The electric field of a single photon is most logically associated with a radial vector at the instantaneous packet locus of the excitation. For a suitably large number of photons on a plane polarized beam, the angular distribution of these vectors may be associated with a radial vector at each of the packets on each of an ensemble's members (see Fig. 2). Symmetry ensures that the vector sum in Euclidean space is a resultant that lies along the centroid of the ensemble. We identify that resultant vector with **E**.

Consequently, in free space, even though the locally real representation objectively implies an angular distribution of radial electric field vectors about an incident beam's polarization orientation, the experimentally observable resultant electric field is not distinguishable from the single vector quantity **E** of classical electromagnetics.

Conversely, the analyzer's structure explicitly applies a physical constraint that necessarily confines the electric field of the internally propagating wave to the plane of the analyzer's polarization axis. Consistent with that constraint, we postulate that the locally real wave structure is, likewise, confined to that plane as a superposition of projections of the incident packets in the form of a single superpacket photon $\mathbf{\Phi}_\delta$.

Representation in Euclidean space also provides us with additional insights specifically relating to the formation of the superpacket. We have seen that the transition of an incident photon, with packets arrayed over an angular arc $\Delta_\gamma = \pi/2$, to a condensed δ-form superpacket within an analyzer is critical to the transmission outcome. From the perspective of the photon's wave structure, the interception or noninterception of the polarization axis by the Δ_γ is of minor consequence. In the example depicted in Fig. 1(b), if we orient the analyzer's polarization axis along the x axis, Δ_γ happens to be intercepted and a large amplitude δ-form superpacket is formed along that axis from the projected components of the incident packets. Although a very slight counterclockwise rotation of that particular Δ_γ arc would result in its noninterception by the polarization axis, the amplitude coefficient b_δ of the superpacket would be only marginally reduced in magnitude. However, from the perspective of the excitation migrating on the photon wave structure entering analyzer A, the difference between interception and noninterception is of paramount significance.

As the incident wave structure begins to penetrate the analyzer, the amplitude of packets on the Δ_γ arc rapidly diminishes toward zero and, simultaneously, the δ-form superpacket amplitude sharply rises along the polarization axis. When the Δ_γ arc of a particular incident $\mathbf{\Phi}_{\gamma i}$ intercepts the polarization axis, the excitation migrating on the diminishing packets of the arc entering the analyzer promptly locks into the rising δ-form superpacket located on Δ_γ and is transmitted through the analyzer as a superpacket photon $\mathbf{\Phi}_\delta$.

Conversely, when the Δ_γ arc of a particular $\mathbf{\Phi}_{\gamma i}$ does not intersect the analyzer's polarization axis, the excitation migrating on the diminishing packets of Δ_γ does not encounter the δ-form superpacket since it is not contiguous with Δ_γ. As a result, the excitation is absorbed in the analyzer and the superpacket on the polarization axis is transmitted as an ''empty wave'' through the analyzer. The ''empty wave'' is equivalent to an excitationless superpacket wave structure $\mathbf{\Phi}_\delta^0$ propagating within the analyzer. We will reserve the term ''photon'' for wave structures that are excitation bearing. At the exit face a full complement excitationless empty wave

ensemble member $\mathbf{\Phi}_\gamma^0$ is emitted. When considering discrete photon phenomena involving two-channel devices such as calcite polarization analyzers and beam splitters, quantities of the form $\mathbf{\Phi}_\gamma^0$ and (a ''photon'') $\mathbf{\Phi}_\gamma$ are emitted, respectively, from the two channels and may subsequently intersect to produce an interference. These quantities immediately provide the means for self-consistently constructing a locally real representation fully inclusive of such two-channel phenomena. Quantum mechanically, such phenomena invoke spatially separated superposition states with nonlocal consequences.

The representation in Euclidean space also allows us to compute changes in the amplitude coefficient as a photon enters and exits an analyzer. When a δ-form superpacket photon reaches the analyzer's exit face, a stochastic analyzer emission process occurs. As a transition from the emergent $\mathbf{\Phi}_\delta$, a photon $\mathbf{\Phi}_\gamma$ is emitted with a $\Delta_\gamma = \pi/2$ packet arc, an orientation of some θ_γ, and a b_γ amplitude coefficient. Aside from the specification of b_γ, that emitted photon is equivalent to one of the members of an ensemble centered about the analyzer's polarization axis selected here as the x axis. We want to understand the role of the packet amplitude coefficient in the context of analyzer transmission processes.

It is easily demonstrated that the amplitude coefficient b_γ of the emitted photon $\mathbf{\Phi}_\gamma$ is a function of that photon's orientation θ_γ and the amplitude coefficient of the superpacket b_δ from which it was generated. Consistent with the analysis applied to Eqs. (14) and (15), the projection of the superpacket amplitude vector along θ_γ has a magnitude $b_\delta \cos\theta_\gamma$. The vector sum of the emitted photon's packet amplitudes produces a resultant vector oriented at this θ_γ with magnitude $M_\gamma = \sqrt{2} b_\gamma / \delta$. Equating these magnitudes uniquely determines the relationship between the objective orientations and amplitudes of the incident and the emitted photons,

$$b_\gamma = \delta b_\delta (\cos\theta_\gamma)/\sqrt{2} = b_{\gamma i} \cos\theta_{\gamma i} \cos\theta_\gamma . \tag{18}$$

Projectively, the analyzer emission process is recognized as a reversal of the condensation process with the explicit reminder in Eq. (18) that the orientations of the incident photon and the emitted photon are not generally equal.

Despite the Eq. (18) dependence of the wave packet amplitude coefficient on the photon orientation values, the physical role of the amplitude coefficient is not pertinent to photon transmission probability through an analyzer where only Δ_γ interception by the polarization axis is relevant.

We see from Eq. (18) that, in general, the amplitude coefficient b_γ is diminished each time a photon enters and exits an analyzer, thereby rescaling the complete wave function $\Phi(z,t;\Delta_\gamma,\theta_\gamma,b_\gamma)$. Similarly, b_γ^2 is also diminished and proportionately rescales the ''wave intensity'' $\Phi^*\Phi$. Since the probabilities of photon analyzer transmission and excitation locus on that photon's wave structure are independent of any rescaling, we are free to suppress b_γ. This suppression effectively renormalizes the intensity each time the photon passes through an analyzer and confers upon $\Phi^*\Phi$ an equivalency to a true mathematical probability. This is certainly a calculational convenience, but we must not lose sight of the wave as a physically real entity.

Before concluding our treatment of analyzer emission processes, we want to note that the polar coordinate θ used above in the construction of ensemble states from a generator photon γ_g at $\theta = 0$ also represented angular positions with respect to the analyzer's polarization axis. We now introduce the angular coordinate Θ to define the physical orientation of an analyzer in the laboratory frame. Choosing Θ as the angle with respect to the polarization axis gives the equivalence $\Theta = \theta$. To that extent, the introduction of Θ may be regarded as superfluous in the treatment of analyzer emission; however, in the context of correlated photons (and correlated particles), we shall need to distinguish the two quantities.

Finally, before leaving the topic of photon analyzer emission, we may reasonably ask why the locally real representation is of utility if we get Malus's law from quantum mechanics as well. The response to this point is that quantum mechanics, aside from Bohm's particular interpretation [26], has already required that we abandon the notion of physical reality for the photon. An even more compelling differentiation between the two representations will occur when we consider correlated states. Quantum mechanics, including the Bohm interpretation, will impose nonlocality.

C. Correlated photons

We consider here atomic transitions emitting two correlated photons that together carry a net angular momentum of zero. The polarization states of the two photons are then π out of phase, but this phase differential is not evidenced by the analyzers and quantum mechanically we expect that both photons are either vertically polarized or horizontally polarized.

In analogy to analyzer emission, a correlated photon pair is treated as an ''independent'' γ_G generator photon and a ''dependent'' γ_E emission photon. The emission photon γ_E is a member of an ensemble $\{\gamma_E\}$, and we require zero angular momentum within the closed system of any γ_G, γ_E correlated pair. To the extent that γ_g and γ_G both generate an ensemble member, the analyzer emission process for $\{\gamma_e\}$ and the correlated photon emission process for $\{\gamma_E\}$ are similar. However, the physical constraints associated with the two processes are different.

A significant difference relates to the photon arc span Δ_γ. In analyzer emission, projections from the γ_g angularly confined δ-form ''source'' yield a $\cos^2\theta$ distribution of $\{\gamma_e\}$ packets. In contrast, the ''independent'' γ_G of a correlated pair is unrestricted by confinement to an analyzer. Accordingly, γ_G is a full complement photon with $\Delta_\gamma = \pi/2$ and presents a generator source that is extended over its entire $\pi/2$ arc of packets.

An additional difference between the analyzer emission process and the correlated photon process is associated with the relevant reference frames. Analyzer emission is most appropriately represented in the laboratory reference frame since the state vector of γ_g is aligned with the polarization axis of the analyzer. Conversely, the orientation of the independent correlated photon γ_G can assume any value at random in the laboratory frame for a particular event in free space. Consequently, it is convenient to translate to the pho-

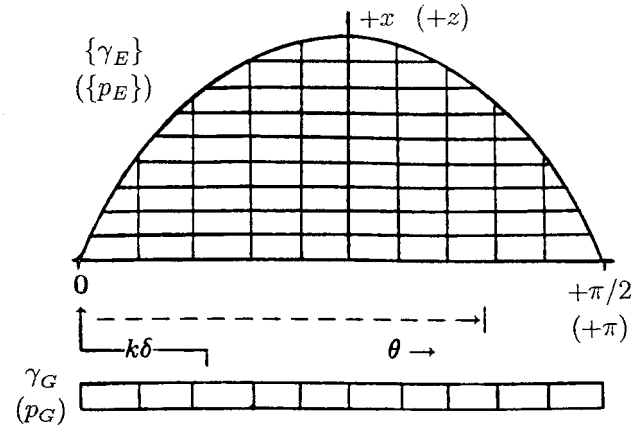

FIG. 3. Correlated photon pair planar wave packets for γ_G and for ensemble members (rows) of $\{\gamma_E\}$. Alternatively, substituting quantities in parentheses gives correlated particle pair spin wave packets for p_G and ensemble members (rows) of $\{p_E\}$.

ton reference frame $K(\theta)$ in which the planar packets of all γ_G photons are always in some fixed orientation relative to θ. Initially, we shall find it convenient to align the exterior wave packets of γ_G with $\theta=0$ and $\pi/2$ as shown in Fig. 3. Subsequently, we will rotationally translate $\theta=0$ to the γ_G bisector (γ_G's *orientation*) defined as $+x$ in K. In either case, with the correlated photon source interposed between a pair of opposed polarization analyzers, the orientations of those analyzers must be treated as completely random in K, constrained only by their fixed relative rotation designated by the angular variable Θ in the laboratory frame.

We shall see that the analyzer transmission results for our present consideration of correlated photons are independent of the amplitude coefficient b_γ. A corresponding independence was observed earlier with respect to transmission of the full complement analyzer emission photons. As a result, we will reexamine the role of b_γ in the context of correlated photons only very briefly in the interests of verifying this independence.

Our principal objective here is to generalize the basic projective formalism of Eqs. (1)–(6) in a consistent manner over the extended γ_G generator source. For every packet location along the angularly extended γ_G source packets, we must project a contribution to the distribution of emission packets in $\{\gamma_E\}$ through all possible angles $\theta=k\delta$. The operation is conducted in $K(\theta)$ as shown in Fig. 3. The projection angle $\theta=0$ $(k=0)$ imposes the boundary condition that $\{\gamma_E\}$ be identically zero outside the arc of γ_G packets where $\theta > \pi/2$ since γ_G is itself zero in this range. Zero angular momentum for all correlated pairs could not be satisfied if $\{\gamma_E\}$ were to exceed this boundary condition. (This condition results in transmission of any $\{\gamma_E\}$ member always being accompanied by transmission of γ_G when the respective analyzers have identical orientations, i.e., $\Theta=0$.)

In the interests of presenting a lucid and explicit derivation of local reality, we shall first consider an approximation of correlated photon structure in a suitably finite dimensional Hilbert space before proceeding to the exact solutions in an infinite dimensional Hilbert space. This approximation allows us to individually enumerate all of the relevant probability outcomes. In this regard, we diverge from the continuum limit of $\delta\rightarrow 0$ and initially examine a coarse $\delta=30°$ example.

The choice of $\delta=30°$ temporarily places us in a six-dimensional Hilbert space since the basis vectors must span an arc of π. As $\delta\rightarrow 0$, the dimensionality of the requisite Hilbert space remains finite at some $2N=\pi/\delta$. Ultimately, when we impose the limit $\delta\rightarrow 0$ on the locally real representation, the dimensionality of the Hilbert space becomes infinite in contrast to the corresponding two-dimensionality of polarization representation in quantum mechanics.

To remind us that we are initially considering the coarsely finite $\delta=30°$ example, angular values are expressed in degrees instead of radians. With $\delta=30°$, three basis vectors in Hilbert space, $|u_1\rangle$, $|u_2\rangle$, and $|u_3\rangle$, span a full complement arc as depicted in Fig. 4. We have the three projections

$$|\phi_1\rangle=c_1|u_1\rangle, \tag{19}$$

$$|\phi_2\rangle=c_1|u_1\rangle+c_2|u_2\rangle, \tag{20}$$

and

$$|\phi_3\rangle=c_1|u_1\rangle+c_2|u_2\rangle+c_3|u_3\rangle. \tag{21}$$

The quantity $|\phi_1\rangle$ is the projection of some correlated photon superposition state $|\phi_E\rangle$ in the Hilbert subspace $|u_1\rangle$. Similarly, $|\phi_2\rangle$ and $|\phi_3\rangle$ are the projections of $|\phi_E\rangle$ in the Hilbert subspaces $|u_1\rangle,|u_2\rangle$ and $|u_1\rangle,|u_2\rangle,|u_3\rangle$, respectively. Note that, because of the multiple generator packets contributing to $|\phi_2\rangle$ and $|\phi_3\rangle$, these vectors are expected to be rotated in Hilbert space away from the $|u_i\rangle$.

For the present set of projections, only in the case of $|\phi_1\rangle$ is there a one to one correspondence between a state vector and the basis vector from which it is constructed. This relationship exists because $|\phi_1\rangle$ arises from a projection of a single generator packet as shown in Fig. 4. Recall that this was the case for every one of the $|\phi_j\rangle$ constituent state vectors of the $|\phi_e\rangle$ analyzer emission superposition state since all projections arose from the single generator photon γ_g.

However, the remaining Eqs. (20) and (21) state vectors are each composed of a mixture of projections from multiple generator packets, two for $|\phi_2\rangle$ and three for $|\phi_3\rangle$. Because of this mixing and because the final state vector $|\phi_3\rangle$ is constructed over a set of basis vectors $|u_1\rangle$, $|u_2\rangle$, and $|u_3\rangle$ that constitute a full complement of packets, we identify the correlated photon superposition state

$$|\phi_E\rangle=|\phi_3\rangle=\sum_{j=1}^{3} c_j|u_j\rangle. \tag{22}$$

As a consequence of the mixing, the c_j coefficients must be extracted from the simultaneous set of Eqs. (19)–(21). We can solve for these values by observing that, as in Eq. (3) for analyzer emission, packet projection from a single generator site through $k\delta$ in Hilbert space yields a projected state vector with norm $\|\phi_k\|=\cos(k\delta)$. From Fig. 4, $|\phi_1\rangle$ is constructed from the 60° projection of the generator packet at

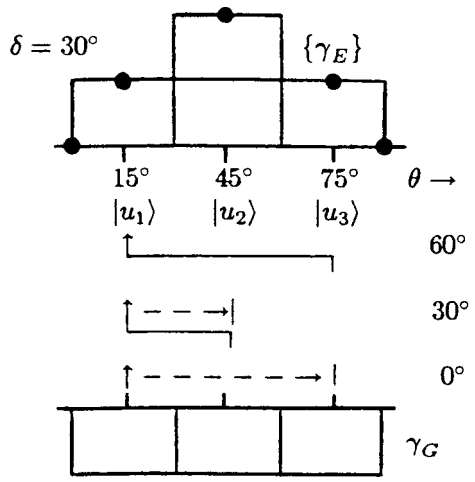

FIG. 4. Correlated photon example for $\delta=30°$ of ensemble planar wave packet projection computation. Joint transmission is 4/4, 3/4, 1/4, and 0/4 when analyzers are relatively rotated by 0°, 30°, 60°, and 90°, respectively.

$|u_3\rangle$. Similar constructions apply to $|\phi_2\rangle$ and to $|\phi_3\rangle$ except that these states are formed from multiple projection contributions. The state vector $|\phi_2\rangle$ is constructed from the 30° projections of generator packets at $|u_2\rangle$ and $|u_3\rangle$, and $|\phi_3\rangle$ is constructed from the 0° projections of generator packets at $|u_1\rangle$, $|u_2\rangle$, and $|u_3\rangle$. Then

$$\|\phi_1\|=\langle\phi_1|\phi_1\rangle^{1/2}=(c_1^2)^{1/2}=\cos 60°=\frac{1}{2}, \tag{23}$$

$$\|\phi_2\|=\langle\phi_2|\phi_2\rangle^{1/2}=(c_1^2+c_2^2)^{1/2}=\cos 30°=\frac{\sqrt{3}}{2}, \tag{24}$$

and

$$\|\phi_3\|=\langle\phi_3|\phi_3\rangle^{1/2}=(c_1^2+c_2^2+c_3^2)^{1/2}=\cos 0°=1. \tag{25}$$

We have from Eqs. (23)–(25)

$$c_1=c_3=\frac{1}{2}, \quad c_2=\frac{1}{\sqrt{2}}. \tag{26}$$

The resultant correlated photon superposition state is

$$|\phi_E\rangle=|\phi_3\rangle=\frac{1}{2}|u_1\rangle+\frac{1}{\sqrt{2}}|u_2\rangle+\frac{1}{2}|u_3\rangle. \tag{27}$$

The coefficients are the amplitudes of $|\phi_j\rangle$ (or equivalently of $|\phi_E\rangle$) along the $|u_j\rangle$. That is,

$$\langle u_1|\phi_1\rangle=\langle u_1|\phi_E\rangle=\cos 60°, \tag{28}$$

$$\langle u_2|\phi_2\rangle=\langle u_2|\phi_E\rangle=\cos 45°, \tag{29}$$

and

$$\langle u_3|\phi_3\rangle=\langle u_3|\phi_E\rangle=\cos 60°. \tag{30}$$

We see that $|\phi_E\rangle$ in Hilbert space is rotated 60° from $|u_1\rangle$, 45° from $|u_2\rangle$, and 60° from $|u_3\rangle$, which is why $|\phi_E\rangle$ has nonzero amplitudes along each of the $|u_j\rangle$.

In order to determine the relative proportion of ensemble packets at the $|u_j\rangle$, we need to calculate the squared amplitudes $\langle u_j|\phi_E\rangle^2$. We have

$$\langle u_1|\phi_E\rangle^2=\langle u_3|\phi_E\rangle^2=\frac{1}{4}, \quad \langle u_2|\phi_E\rangle^2=\frac{1}{2}. \tag{31}$$

For the particular example of $\delta=30°$, the Eq. (31) values express the relative probabilities of correlated photon ensemble packets at each $|u_i\rangle$ as depicted in Fig. 4. As previously observed, the ensemble packet probability is immediately equivalent to the ensemble packet distribution for photons. We can then readily determine the requisite packet configurations of ensemble members from the Fig. 4 packet *distribution*. The lower packet row of $\{\gamma_E\}$ is identified as a full complement ensemble member γ_{E1}. Symmetry about the bisector axis of that member and the γ_G provides the requisite zero net angular momentum for the γ_{E1},γ_G pair. The remaining single packet in the upper row of $\{\gamma_E\}$ is necessarily identified as the other ensemble member γ_{E2}. Symmetry still preserves the requisite zero net angular momentum for the γ_{E2},γ_G pair. We see that the single packet γ_{E2}, with a total arc span $\Delta_\gamma=30°$ instead of the full complement $\Delta_\gamma=90°$, is a natural and necessary outcome of the ensemble construction in Hilbert space.

Despite the coarseness of $\delta=30°$, this example proves to be nontrivially informative, and it is instructive to examine the predicted measurement outcomes before proceeding to the limit of $\delta\to 0$. We can readily enumerate all of the joint transmission probabilities $P_\gamma(k\delta)$ by inspection of the packet ensemble distribution in Fig. 4 when the opposed analyzers have the relative angular separations of $\Theta=0°$, 30°, 60°, and 90°. We begin with $P_\gamma(0°)$ which is a summation of the 0° samplings in Fig. 4, i.e., both analyzers intersect γ_G and $\{\gamma_E\}$ at the same $|u_i\rangle$. We have

$$P_\gamma(0°)=\frac{1}{12}(1+2+1+3\times 0). \tag{32}$$

The 1/12 factor is the requisite normalization for the total number of samplings. These include the three samplings associated with $|u_1\rangle$, $|u_2\rangle$, and $|u_3\rangle$ which intersect γ_G and $\{\gamma_E\}$. Additionally, we must include the three additional samplings at $|u_4\rangle$, $|u_5\rangle$, and $|u_6\rangle$ for which neither γ_G or $\{\gamma_E\}$ are intersected. These six samplings must be doubled to 12 because there are two ensemble members. The first three terms in the factor in parentheses give the summation of the ensemble packets at $|u_1\rangle$, $|u_2\rangle$, and $|u_3\rangle$ for which a γ_G packet is correspondingly always intersected. The 3×0 term reflects the noninterception of both γ_G and $\{\gamma_E\}$ for $|u_4\rangle$, $|u_5\rangle$, and $|u_6\rangle$.

Similarly, $P_\gamma(30°)$ is computed from the 30° offset of analyzer orientations as shown in Fig. 4 and we have

$$P_\gamma(30°)=\frac{1}{12}(1+2+4\times 0). \tag{33}$$

Since we are computing joint transmission, the zeros in parentheses include sampling nonintersection with both γ_G and $\{\gamma_E\}$ as well as nonintersection with either γ_G or $\{\gamma_E\}$. By the same process we have

$$P_\gamma(60°)=\frac{1}{12}(1+5\times 0),\quad P_\gamma(90°)=\frac{1}{12}(6\times 0). \tag{34}$$

All of these joint transmission probabilities can be compactly expressed in terms of the squared Eq. (31) amplitudes, giving

$$P_\gamma(k\delta)=\frac{4}{12}\sum_{i=1}^{3-k}\langle u_i|\phi_E\rangle^2=\frac{1}{2}\left(\frac{2}{3}\right)\sum_{i=1}^{3-k}c_i^2=\frac{1}{2}\left(\frac{2}{3}\right)\cos^2(k\delta). \tag{35}$$

We recognize that the extracted $\frac{1}{2}$ factor in Eq. (35) arises from the γ_G occupying half of the complete set of Hilbert space unit vectors $|u_1\rangle,\ldots,|u_6\rangle$. The extracted $\frac{2}{3}$ factor is defined as the *fractional occupancy* F_γ of packets in the $|u_1\rangle,|u_2\rangle,|u_3\rangle$ subspace of the ensemble distribution, Fig. 4. This fractional occupancy arises naturally from the construction of the correlated photon superposition state $|\phi_E\rangle$ and has profound implications with regard to the applicability of Bell's theorem [4,25]. Because of this fractional packet occupancy, a γ_G transmission is accompanied by a γ_E transmission only two-thirds of the time when the analyzers are aligned $(k=0)$. Equivalently, the average arc span of an ensemble member is

$$\langle\Delta_\gamma\rangle=F_\gamma 90°=\frac{\frac{1}{2}(90°+30°)}{90°}90°=60°, \tag{36}$$

which is two-thirds of a full complement $\Delta_\gamma=90°$. However, because of the coarseness of the $\delta=30°$ example, the two-thirds fractional occupancy of the ensemble packet distribution converges to a modified value as $\delta\to 0$. We shall reexamine the significance of the fractional packet occupancy factor F_γ after taking this limit.

Finally, before leaving the $\delta=30°$ example, we observe that the normalized ensemble packet distribution can be fitted to a $\sin(2\theta)$ function at the five indicated points shown in Fig. 4.

As $\delta\to 0$, the number of Hilbert space orthonormal basis vectors spanning a $\Delta_\gamma=\pi/2$ full complement arc increases from the present three (for $\delta=30°$) to some $N=\pi/(2\delta)$. The Hilbert space increases from six dimensional to $2N$ dimensional. The construction of $|\phi_1\rangle$ through $|\phi_N\rangle$ proceeds as before, yielding a set of N readily solvable simultaneous equations in diagonal form analogous to Eqs. (23)–(25). Equation (35) becomes

$$P_\gamma(k\delta)=\frac{1}{2}F_\gamma\sum_{i=1}^{N-k}\langle u_i|\phi_E\rangle^2=\frac{1}{2}F_\gamma\cos^2(k\delta), \tag{37}$$

giving the joint transmission probabilities for any integer value of $k=\Theta/\delta$. The exact value of F_γ can be determined from Eq. (37) for sufficiently large N. However, we shall obtain F_γ below after converting the summation to an integral equation as we reach the limit $\delta\to 0$.

The integral form of Eq. (37) is

$$P_\gamma(\Theta)=\frac{1}{2}F_\gamma\int_0^{\pi/2-\Theta}E_\gamma(\theta)d\theta=\frac{1}{2}F_\gamma\cos^2\Theta, \tag{38}$$

for which the ensemble packet distribution is given by the function $E_\gamma(\theta)$. The solution of this integral equation is $E_\gamma(\theta)=\sin 2\theta$, and we can now identify this solution with the packet ensemble envelope of $\{\gamma_E\}$ depicted in Fig. 3. The packet occupancy fraction is

$$F_\gamma=\frac{\int_0^{\pi/2}\sin(2\theta)d\theta}{\int_0^{\pi/2}d\theta}=\frac{2}{\pi} \tag{39}$$

and demonstrates that the packet occupation fraction F_γ diminishes from 2/3 for $\delta=30°$ to $2/\pi$ for $\delta\to 0$.

Then the joint transmission probability in the limit $\delta\to 0$ is

$$P_\gamma(\Theta)=\frac{1}{\pi}\cos^2\Theta. \tag{40}$$

At this point, we apply a $\pi/4$ rotational translation of $\theta=0$ in $K(\theta)$ thereby aligning the bisector (orientation) of γ_G with the defined axis x noted in Fig. 3. Under this translation, the envelope of ensemble packets $E_\gamma(\theta)=\cos 2\theta$ and the γ_G packets are symmetrized about x without altering $P_\gamma(\Theta)$.

We can now proceed with the construction of the emission ensemble members $\{\gamma_E\}$ from the Fig. 3 distribution of ensemble packets. This process is a trivial extension of the $\delta=30°$ example. Zero net angular momentum for all γ_G,γ_E correlated pairs and packet contiguity require identification of the Fig. 3 packet rows as the constituent $\{\gamma_E\}$ members. These $\{\gamma_E\}$ members have a continuous spectrum of arc spans ranging from zero to $\pi/2$. The packet occupation fraction gives an average ensemble member arc span of

$$\langle\Delta_\gamma\rangle=F_\gamma\frac{\pi}{2}=1. \tag{41}$$

For any particular correlated photon pair, the γ_E is a random member (row) of the emission ensemble $\{\gamma_E\}$. The γ_E and its associated γ_G share an orientation θ_γ that is random in the laboratory frame and is identically zero in K.

In order to calculate the predicted "joint probability" $\wp_\gamma(\Theta)$ for detectors placed beyond each of the analyzers we need to derive expressions for the coincidence rates $R(\Theta)$ with analyzers (relatively rotated by Θ) and R_0 without analyzers. We have

$$R(\Theta)=R_T f P_\gamma(\Theta)\eta^2 \tag{42}$$

where R_T is the true production rate of correlated photons from the source and f is the fractional angular acceptance cone of the opposed analyzer-detector sets. The joint trans-

mission probability $P_\gamma(\Theta)$ is given in Eq. (40) and η is the detector efficiency for the analyzer transmitted photons. Correspondingly, without analyzers, the coincidence rate is

$$R_0 = R_T f \eta \langle \eta_E \rangle. \tag{43}$$

The notable feature of this expression is the efficiency $\langle \eta_E \rangle$ associated with the detector intersecting an emission ensemble member. The other detector intercepts the full complement γ_G for which detection efficiency is η.

This photon-specific dependence of detection efficiency is related to the relative interaction cross section of the photon, which is a function of its Δ_γ arc span. As the photon propagates through a detector, the wave frequency mediates the rate at which the excitation migrates to random points along Δ_γ. Accordingly, as the wave progresses a short distance in the detector, the excitation rapidly reaches the entirety of the Δ_γ arc span. (At optical frequencies, the requisite distance is on the order of several micrometers.) Moreover, this distance is further diminished as the phase velocity exceeds the group velocity since the latter gives the average excitation velocity along the propagation axis.

Consequently, the effective cross section of interaction presented to the detector for a given photon is proportionate to that photon's packet arc span Δ_γ. Over the range that a detector exhibits a Δ_γ-proportionate efficiency, the detector's response is defined as having the property of *linearity*. From the averaged Δ_γ values of the $\{\gamma_E\}$ ensemble members, the detection efficiency

$$\langle \eta_E \rangle = F_\gamma \eta = \frac{2}{\pi} \eta. \tag{44}$$

The quantity $\langle \eta_E \rangle$ did not arise in $R(\Theta)$ because the transmission of γ_E through the analyzer is accompanied by the associated packets condensing along polarization axes. The history of the incident γ_E arc span is erased in the process of transmission. The emergent photon is a full complement member of an analyzer emission ensemble $\{\gamma_e\}$ and consequently is detected with an efficiency η. The detection efficiency of the γ_E photons is naturally ''enhanced'' in the process of transmission through an analyzer. It may be readily appreciated that these results are independent of the amplitude coefficient b_γ. This independence is consistent with the analyzer interaction phenomenon we considered earlier.

The ratio of the Eqs. (42) and (43) coincidence rates gives the expression for the ''joint probability''

$$\wp_\gamma(\Theta) = \frac{R(\Theta)}{R_0} = \frac{R_T f P_\gamma(\Theta) \eta^2}{R_T f \eta \langle \eta_E \rangle} = \frac{1}{2} \cos^2 \Theta. \tag{45}$$

We then have agreement between the locally real representation and quantum mechanics. This outcome clearly depends upon the linearity of the detector's efficiency with respect to the intercepted photon's arc span as expressed in Eq. (44). The property of linearity is compatible with ''low efficiency'' detectors. Nevertheless, the range of linearity is bounded and detectors beyond that boundary are predicted to yield a joint probability different from that of Eq. (45). This predicted difference was considered earlier [24].

More specifically, the locally real representation predicts that the Eq. (45) result is necessarily violated only when $\langle \eta_E \rangle > 2/\pi$ (63.7%) since linearity would require $\eta > 1$ for full complement photons. Equivalently, the detector efficiency must exceed the efficiency

$$\langle \eta_m \rangle = \frac{1}{2}\left(\frac{2}{\pi} + 1\right) \approx 81.8\% \tag{46}$$

for an equal population mixture of γ_E's and full complement γ_G's. Equation (46) demonstrates that the locally real representation presented here is testable with respect to quantum mechanics.

If linearity is maintained up to the maximum limit of $\langle \eta_E \rangle$, then the predicted difference must manifest itself as a convergence of the 1/2 coefficient in Eq. (45) to $1/\pi$ as $\langle \eta_E \rangle$ progresses from $2/\pi$ to 1 while η remains at 1.

However, it should be stressed that the Eq. (45) result, which is in agreement with quantum mechanics, remains consistent even with presently available detectors commonly regarded as ''high efficiency.'' For example, a detector with a 90% efficiency for full complement photons would, by linearity, be expected to exhibit an average $(2/\pi)90\% \approx 57.3\%$ efficiency for the $\{\gamma_E\}$ ensemble members and, with $\langle \eta_m \rangle \approx 73.6\%$, the Eq. (46) condition is not exceeded.

III. LOCALLY REAL PARTICLE STATES

A. Introduction to particle states

We consider here the construction of locally real particle states in analogy to those of photons. We will examine spin $\frac{1}{2}$ particles, but our results are readily extendable to particles of different spin composition.

The construction begins in the rest frame of a particle with the fundamental entity of a *spin packet* defined on the vacuum field of oscillators in random ground state motion. A spin packet is characterized by rotational coherence of ground state oscillator motion in a plane about some specified point as depicted in Fig. 5(a). That point can be selected as the origin of a coordinate frame. A bivector **s**, extending from the origin and normal to the rotational plane, specifies the orientation and sense of rotation of the spin packet. The intersection of the particular bivector **s** on the unit sphere designates an infinitesimal conic intersection area or, equivalently, a solid angle a_δ. The planar infinitesimal angular arc δ of a_δ is of particular utility and, in relation to the spin packet, is functionally analogous to the δ quantity for a planar wave packet with respect to the construction of particle states.

The set of all variously oriented spin packets at a common point map their associated a_δ to cover a zone on the unit sphere and collectively define a *spin structure*. (The zones we shall be considering are defined as the spherical surface between a plane transecting the unit sphere and a parallel plane tangent to the sphere. The point of tangency defines the pole of the zone. The orientation of this pole is a critical specification.) The phase of the rotational coherence is the

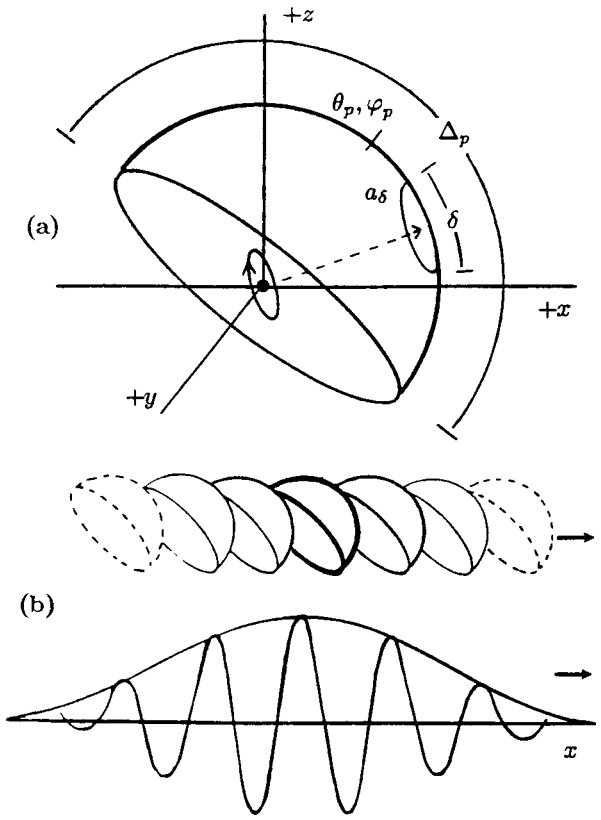

FIG. 5. Schematic representation of spin $\frac{1}{2}$ particle. For a constituent (a) spin structure, a rotational oscillator coherence at the origin constitutes a spin wave packet characterized by a bivector intersecting the unit sphere over some a_δ solid angle. Only a single typical spin wave packet is depicted. The set of all spin wave packets covers a spherical zone of planar arc span Δ_p that defines the spin structure. A particle propagating along an axis (x) consists of (b) a sequence of spin structures with fixed orientation but varying in rotational phase and coherent oscillator density (collectively scaled by an amplitude coefficient b_p).

same on all spin packets of a particular spin structure. The specification of a particular spin structure includes the associated zone's total planar arc Δ_p and the zone's pole orientation θ_p, φ_p in spherical coordinates. These three quantities are *field variables* of a particle. For a *full complement* spin $\frac{1}{2}$ particle, the solid angle of the spin structure's zone is 2π, giving a planar arc $\Delta_p = \pi$.

We shall have frequent occasion to consider here particles emitted from a *source* such as a Stern-Gerlach analyzer. As a particle is emitted, the spin structure is replicated along the propagation axis as shown schematically in Fig. 5(b). These spin structures are all identical with respect to a particular particle's fixed values of the $\Delta_p, \theta_p, \varphi_p$ field variables. However, the phase of the spin structures varies along the propagation axis chosen here as x. An amplitude coefficient b_p constitutes an additional field variable that scales the amplitude of the physically realized spin structures. Additionally, there is typically a dispersion of values for canonically conjugate variables such as x and p_x (the momentum component on x). Superposition over this dispersion for constituent waves yields a relative density of coherently moving oscillators on the individual spin structures that varies as a function of x. These variations in the spin structures along x are given by the configuration space wave function $\Psi(x,t)$ on $t \geqslant 0$ associated with the standard quantum formalism (but not with its probabilistic interpretation).

We then identify Ψ as the descriptor of relative phase on these spin structures as a function of x. The envelope $\Psi^*\Psi$ provides a measure of the density of coherently moving oscillators on particular spin structures again as a function of x. The density over the entire envelope is scaled by a factor of b_p^2.

The set of these spin structures constitutes the total wave structure of a particular particle. In the locally real representation, we are reminded that, for a particular particle, the field variables $\Delta_p, \theta_p, \varphi_p$ as well as b_p are some fixed values the instant emission occurs and functionally $\Psi_{t\geqslant 0} = \Psi(x,t;\Delta_p, \theta_p, \varphi_p, b_p)$. This total wave structure together with an excitation state, instantaneously residing on one of the spin packets located on one of the spin structures, specifies that particular particle. The excitation migrates on the coherently moving oscillators of this wave structure with a relative probability along the set of spin structures given by $\Psi^*\Psi$ and a random probability on any particular spin packet of the spin structure on which it instantaneously resides. As with photons, both of these probabilities as well as analyzer transmission probabilities are independent of the amplitude coefficient b_p. The primary benefit derived from considering b_p in the present context of single channel analyzers is only to emphasize that the wave structure of a particle is a real scalable entity.

We have then a general physical representation of the particle that is closely analogous to that of the photon. Measurements of canonically conjugate variables such as x and p_x on a large number of similarly generated particles effectively sample the instantaneous values of those variables assumed by the excitation on those particles. The collective set of such measurements can, for example, reconstruct the envelope of $\Psi^*(x,t)\Psi(x,t)$ in configuration space since this envelope is essentially identical for all of the similarly generated particles aside from the scale factor introduced by b_p^2. That scale factor does not alter the relative probabilities of the excitation on a particle's wave structure.

As with photons, the relationship of Δx and Δp_x uncertainties obtained from a collective set of measurements on the canonically conjugate x and p_x variables is a consequence of the classical uncertainty associated with real waves in their composition from harmonic waves expressed in dispersions of those variables.

The specification of a particular emitted particle's spin, however, is given by fixed values of the field variables $\Delta_p, \theta_p, \varphi_p$. We shall demonstrate the spin measurement outcome for particles as a function of these variables in close analogy to photon polarization measurement, but our primary task will be to derive the formalism that assigns the fixed values of these field variables to the emitted particles. This derivation for particles follows consistently from that of photons.

The formalism we seek generates a wave function ψ at the emission source for $t<0$. An ensemble of particles having the proper frequency distribution of the allowable Δ_p and θ_p values is specified by ψ (and the spherical coordinate angle φ_p assumes a random value on $[0,2\pi]$ in our present representation). In a stochastic process at $t=0$, a random ensemble member described by $\Psi(x,t;\Delta_p,\theta_p,\varphi_p)$ is emitted with fixed Δ_p and θ_p,φ_p values.

The emitted particle also has some particular value of amplitude coefficient b_p. However, as with b_γ for photons, the value of b_p is not directly related to the process of constructing ensemble states which is our principal objective. In further analogy with photon states, the excitation probability on the particle's wave structure and the particle's transmission probability through an analyzer are both independent of b_p. The primary remaining benefits derived from considering b_p in the present context of single channel analyzers are only to further emphasize that the wave structure of a particle is a real scalable entity and to gain some measure of physical insight into particle structure and analyzer interaction. Since the close analogs to these subjects have both been explored in our treatment of photon states, we will forego here any similar extensive examination for b_p.

B. Analyzer emission of particles

The Stern-Gerlach analyzer for spin $\frac{1}{2}$ fermions is a two-channel analyzer. The present treatment of analyzer emission and correlated particles requires only consideration of single channel transmission with the other channel blocked. As with our treatment of photon analyzer emission and correlated photons, we defer a more detailed consideration of (spin) packet transmission in analyzers with both channels open to a subsequent treatment that provides a locally real representation of quantum mechanical spatially separated superposition states.

We begin with a randomly oriented full complement particle incident on an analyzer with a single open channel. For random choices of the fixed azimuthal θ_p values, there are $\frac{1}{2}$ probabilities that $\theta_p<\pi/2$ and that $\theta_p>\pi/2$. If we select the analyzer's open channel axis to be along its positive magnetic field $+B=+z$, there is a $\frac{1}{2}$ probability that the particle's spin packet structure will intersect $+z$. When this intersection occurs, spin packets from this structure and the excitation condense to the $+z$ axis (in δ-form analogous to that of photons) and propagate through the analyzer.

Conversely, there is a $\frac{1}{2}$ probability that the spin packet structure will intercept the analyzer's $-z$ axis. In this case the excitation is absorbed as it proceeds along the blocked channel while residing on the spin packets condensed on $-z$ and no detectable particle emerges. (Nevertheless, spin packets still condense along the $+z$ axis and an ''empty wave'' ensemble member is emitted by the open channel.)

For the transmission case, we designate the δ-form particle propagating in the analyzer as the *generator particle* p_g. As p_g emerges from the analyzer, its δ-form spin packet along $+z$ [associated with the basis vector $|v_0\rangle$ in a $2N$ $(=2\pi/\delta)$ dimensional Hilbert space] generates a set of ensemble emission state vectors

$$|\psi_k\rangle=\cos\left(\frac{k\delta}{2}\right)|v_k\rangle. \tag{47}$$

The set of $|v_k\rangle$ are orthonormal basis vectors associated, respectively, with $\theta=k\delta$ for integer values of k where $|k\delta|\leqslant\pi$. The half-angle cosine factor in Eq. (47) gives the appropriate coefficient for the rotational projection of a bivector quantity such as the spin packet. (The associated Hilbert space becomes infinite dimensional when we ultimately take the limit $\delta\rightarrow 0$.)

The amplitude of a projection state vector $|\psi_k\rangle$ is

$$\langle v_k|\psi_k\rangle=\cos\left(\frac{k\delta}{2}\right) \tag{48}$$

and is equivalent to the norm of $|\psi_k\rangle$,

$$\|\psi_k\|=\langle\psi_k|\psi_k\rangle^{1/2}=\cos\left(\frac{k\delta}{2}\right). \tag{49}$$

The probability of an ensemble spin packet at $|v_k\rangle$ is given by the squared amplitude

$$\langle v_k|\psi_k\rangle^2=\cos^2\left(\frac{k\delta}{2}\right). \tag{50}$$

Through the projective process, the right side of Fig. 2 (i.e., $\theta\geqslant 0$) is the azimuthal spin packet probability in any plane inclusive of the magnetic field axis $+B=+z$ upon applying the alternative quantities in parentheses in the figure. This plane can be chosen as xz without loss of generality. In spherical coordinates, the azimuthal dependence can be defined entirely on the positive value range $[0,\pi]$. However, in the present case we can reflect the spin packet probability about the $+z$ axis. From this reflection, we obtain an unaltered $\cos^2(\theta/2)$ spin packet probability in the xz plane where θ, now as a polar coordinate about z, can assume positive and negative values in close analogy to the role of θ in the photon's planar wave packet probability. Figure 2 is then dually applicable to photon analyzer emission processes and, upon applying the alternative quantities, to particle analyzer emission processes.

Similarly, we can also invert the $\theta<0$ contour without altering the spin packet probability in the xz plane. The particle's spin packet probability contour with this modification is, likewise, closely analogous to the photon's planar wave packet probability following a comparable inversion.

There is, nevertheless, a significant distinction between the packet probabilities of photons and of particles. The complete set of the photon ensemble planar packets associated with polarization analyzer emission lie entirely in the plane orthogonal to the propagation axis. Accordingly, Fig. 2 applied to photon analyzer emission, in addition to giving the angular packet probability, also represents the angular distribution of the entire set of planar packets. Additionally, because a complete set is given, the planar packet composition of the $\{\gamma_e\}$ members as the rows of the Fig. 2 modified contour is immediately identifiable.

Conversely, while the Fig. 2 modified contour is also the spin packet probability in any *azimuthal plane* (i.e., a plane inclusive of $+z$), the actual distribution of spin packets is three dimensional and must be discerned from the probabilities. Accordingly, the spin packet rows each correlate respectively with the packet probability of full complement ($\Delta_p = \pi$) ensemble members p_e of $\{p_e\}$. However, the *orientation* of each row is the consequence of rotational averaging of a particular p_e about z (through φ), where we are reminded that the orientation of a row is equivalent to the θ_p bisector angle at the row's center. The p_e orientation prior to rotation is not typically the same as its probability orientation in Fig. 2.

The transformation from a presently unknown distribution of ensemble members to the Fig. 2 probability of ensemble members may be derived from an examination of a single arbitrary $\{p_e\}$ member at some fixed orientation θ_p. We can choose the prerotation plane of that p_e to be xz without loss of generality. Then the zone of p_e is shown in cross section in Fig. 6(a) and the packets of this zone intersected by the xz plane are depicted in Fig. 6(b) as a function of θ.

In order to obtain the associated packet probability, p_e must be rotated about z from its present orientation $\varphi=\pi$ to $\varphi=3\pi/2$ while keeping θ_p fixed. The p_e packets intersected by the xz plane averaged over this rotation give us the packet probability of some specific row in the Fig. 2 modified contour. The transformation, computed for this arbitrary p_e, allows us to map from the $\{p_e\}$ with all members oriented in xz to the (postrotation) packet probabilities of Fig. 2. Note that symmetry allows us to confine the rotation to the $\varphi=[\pi,3\pi/2]$ quadrant of the xy plane. The $\varphi=[\pi/2,\pi]$ quadrant gives a redundant result. Alternatively, if we had selected instead a $\theta_p>0$, a rotation in the $\varphi=[0,\pi/2]$ quadrant would have sufficed.

For calculational purposes, we will leave our arbitrary p_e oriented in the xz plane as in Fig. 6(a) and, instead, perform the requisite rotational averaging by sweeping the vector $\mathbf{r}$ along the base surface of p_e from an azimuthal angle of θ_A at $\varphi=0$ (in the xz plane) to $\varphi=\pi/2$ along the $+y$ axis where the azimuthal angle of $\mathbf{r}$ increases to $\pi/2$ as shown in Fig. 6(c). Clearly, the averaged azimuthal value of $\mathbf{r}$ over this rotation is some angle intermediate between θ_A and $\pi/2$. This value is equivalent to the maximal azimuthal extent θ_B of one of the packet probability rows in the upper half of Fig. 2.

Then, qualitatively, the Fig. 6(a) $p_e(\theta_A)$ ensemble member, with its initial Fig. 6(b) row of xz packets, is displaced (transformed) to the right to θ_B after rotational averaging as indicated in the figure.

We now turn to a quantitative determination of the $\theta_A \rightarrow \theta_B$ transformation. The base of $p_e(\theta_A)$ in Fig. 6(a) along which $\mathbf{r}$ is swept is the plane $x/z=\tan\theta_A$ as defined in Fig. 6(c). After rotation of $\mathbf{r}$ through some φ, we have

$$\tan\theta_C=\frac{z}{L}=\frac{x}{L\tan\theta_A}=\frac{\cos\varphi}{\tan\theta_A}. \tag{51}$$

The complementary angle $\theta_B=\pi/2-\theta_C$ represents the maximal azimuthal extent of $p_e(\theta_A)$ at φ. From Eq. (51)

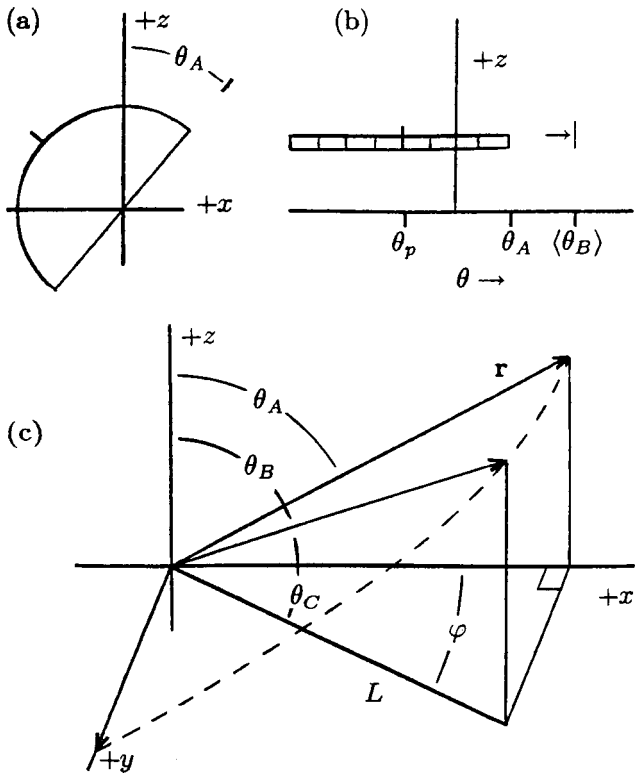

FIG. 6. Spin structure orientation of typical particle ensemble member (analyzer emission) prior to rotational averaging (a) as a zone in xz plane and (b) in corresponding polar angle representation showing $\theta_A \rightarrow \langle\theta_B\rangle$ postaveraging translation. To rotationally average the typical spin structure, (c) sweep $\mathbf{r}$ along zone "base" from xz plane to yz plane.

$$\theta_B(\theta_A,\varphi)=\tan^{-1}\left(\frac{\tan\theta_A}{\cos\varphi}\right) \tag{52}$$

and the probability of θ_B over the entire rotation $\varphi=k\Delta\varphi$ is

$$\begin{aligned}\langle\theta_B\rangle&=\frac{2}{\pi}\sum_{k=0}^{\pi/(2\Delta\varphi)}\theta_B(\theta_A,k\Delta\varphi)\Delta\varphi\\&=\frac{2}{\pi}\int_0^{\pi/2}\theta_B(\theta_A,\varphi)d\varphi\\&=2\cos^{-1}\sqrt{1-\frac{\theta_A}{\pi}}.\end{aligned} \tag{53}$$

We recognize $\langle\theta_B\rangle$ as the maximal extent in θ of the ensemble member packet probability rows in the upper half of Fig. 2. The inverse of Eq. (53),

$$\theta_A=\pi\sin^2\frac{\langle\theta_B\rangle}{2}, \tag{54}$$

gives us a transformation that can be applied to these probability rows to obtain the corresponding (prerotation) maximal θ extent of the ensemble members oriented in the xz plane. Symmetry considerations permit application of this transformation to the entire Fig. 2 modified contour, i.e., the

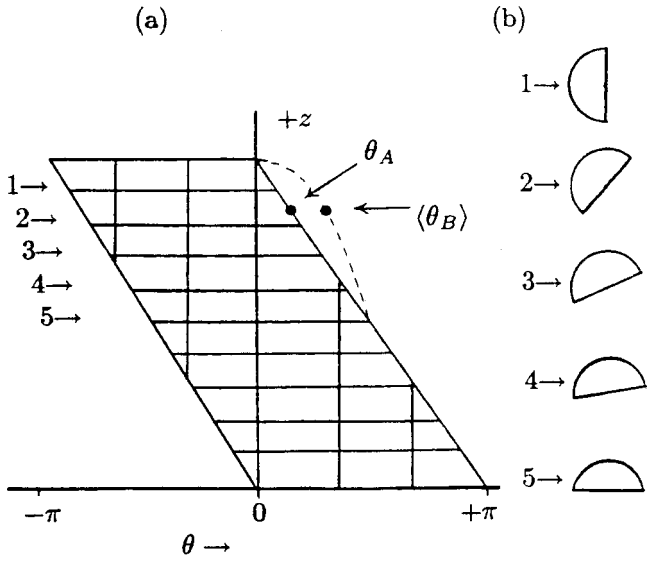

FIG. 7. Analyzer emission ensemble spin packet distribution showing linear θ dependence of member orientations (a) in a polar representation, including postaveraging probability envelope (dashed line) and (b) as a set of zones in the xz plane.

complete θ extent of the members. The cross-sectional distribution of the $\{p_e\}$ ensemble members oriented in the xz plane is shown in Fig. 7(a) as a function of θ. We readily identify the underlying ensemble members as a set of spin structures linearly distributed in θ by the Eq. (53) transformation.

As a consequence of our conversion from azimuthal θ to polar θ, we see that in the final construction of the ensemble members, the upper and lower sets of rows in Fig. 7(a) are mutually redundant. Either set, upon rotational averaging over a full $\varphi=2\pi$, generates an azimuthal (not a polar) angle probability of packets in agreement with the azimuthal probability shown in Fig. 2 for $\theta>0$.

Then, an elegantly simple ensemble consisting of a set of full complement particles with orientations linearly distributed in azimuthal θ over $[0,\pi/2]$ is associated with emission from a Stern-Gerlach analyzer with a single open channel [see Fig. 7(b)]. The members are also randomly distributed in φ over $[0,2\pi]$, but this aspect is not depicted in Fig. 7(b).

For analyzer emission of particles, the laboratory frame angle Θ with respect to the $+z=+B$ axis of the analyzer is identical to θ used in the construction of the ensemble. Similarly, the analyzer's angular orientation in the xy plane of the laboratory frame is $\Phi=\varphi$. Given these equivalences, we can substitute Θ,Φ for θ,φ. The rationale for this substitution is realized when we treat correlated particles for which θ and φ assume the role of integration variables.

A subsequent Stern-Gerlach analyzer A' rotated from A by some azimuthal Θ then serves as an analyzer of the A output. From the construction of the ensemble, we obtain a $\cos^2(\Theta/2)$ probability of transmitting A emission ensemble members through A' in agreement with the probabilistic interpretation of quantum mechanics.

However, in the locally real representation, particles emitted from analyzer A are not probabilistic binary quantum objects with spin up or spin down but are, instead, real entities stochastically selected from $\{p_e\}$. An arbitrary ensemble member p_e has a full complement spin structure with a random orientation over $\Theta=[0,\pi/2]$ and $\Phi=[0,2\pi]$ of some Θ_p,Φ_p $(=\theta_p,\varphi_p)$. At the instant $t=0$ that particle p_e is emitted from A, the outcome is fully determined for transmission through a subsequent Stern-Gerlach analyzer A', rotated azimuthally by Θ at some Φ with respect to A. As with photons, the outcome is independent of the amplitude coefficient.

C. Correlated particles

In our investigation of correlated particles, we consider a process in which a pair of emitted spin $\frac{1}{2}$ particles carry a net angular momentum of zero. The spin states of these particles are then expected to be opposite.

In analogy to analyzer emission of particles and to photon states, a correlated particle pair is identified as an independent generator particle p_G and a dependent emission particle p_E. As in the construction of correlated photon states, p_E is a member of an ensemble $\{p_E\}$.

Also in further close analogy to photons, the generator particle p_g in analyzer emission is physically constrained to a δ-form within the analyzer along the transmission channel axis whereas no such constraint is present for the correlated generator particle p_G which is created as a full complement particle with $\Delta_p=\pi$. This full complement p_G, unlike the δ-form p_g, presents an angularly extended generator source contributing to the construction of $\{p_E\}$ spin packets as shown in the Fig. 3 cross-sectional depiction upon applying the alternative quantities in parentheses.

Furthermore, within the closed system of any p_G,p_E pair emitted in free space, the orientation of the pair is random in the laboratory frame as defined by the pole of, e.g., p_G. As in the case of correlated photons, we find that it is expedient to transform to the particle reference frame K in which p_G has a fixed orientation. Initially, for the convenience of computing projections, we choose to align the spin packet arc span Δ_p of p_G with the angle θ in K spanning 0 to π as shown in Fig. 3. (Later, we will rotationally translate θ as we previously did for correlated photons.)

The correlated particle source is situated between opposed Stern-Gerlach analyzers A_1 and A_2 that have their respective magnetic field $\mathbf{B}_1$ and $\mathbf{B}_2$ vector axes relatively rotated by Θ. Aside from this relative angular displacement, the vectors $\mathbf{B}_1$ and $\mathbf{B}_2$ assume random orientations in K for any particular pair of correlated particles.

Then, Fig. 3 is the probability of spin packets for $\delta\rightarrow 0$ in an arbitrary plane in K, such as xz with θ presently referenced to $+x$, and the rows define the ensemble members transecting that plane. The functional form of the probability envelope is yet to be determined. We must also ascertain the full three-dimensional probability and distribution of the ensemble members and then calculate the Stern-Gerlach analyzer joint transmission probability over the ensemble before finally calculating the joint (detection) probability.

Symmetry properties of the correlated p_G and $\{p_E\}$ members arising from zero net angular momentum require that the xz spin packet probability be maintained upon rotation about $+z$. Accordingly, rotation of the Fig. 3 probability immediately gives the full three-dimensional probability of the ensemble members as a set of coaxial zones oriented at $+z$. Moreover, rotational symmetry imposes equivalence of spin packet probability with spin packet distribution for $\{p_E\}$. We saw that this equivalence was not applicable to $\{p_e\}$.

However, before proceeding with the calculation of the ensemble state vector for this set where we have an infinite dimensional Hilbert space, we temporarily revert to a coarse δ example in order to demonstrate calculation of the ensemble state vector with a finitely countable number of spin packets as we did for correlated photon states. We shall also express angular quantities in degrees as a reminder that we are examining this coarse δ example.

In the particle reference frame K we choose $\delta=60°$, which gives three angular increments for a full complement particle in analogy to the choice of $\delta=30°$ for photons. The corresponding Hilbert space is six dimensional in spanning 360°. For the emission ensemble we have an orthonormal set of basis vectors $|v_1\rangle$, $|v_2\rangle$, and $|v_3\rangle$ in Hilbert space that can be respectively associated with the orientations $+30°$, $+90°$, and $+150°$ in a plane that we can choose as xz without loss of generality. The orientations are defined as polar angles measured from the $+x$ axis.

The respective basis vectors at $|v_4\rangle$, $|v_5\rangle$, and $|v_6\rangle$ are associated with the p_G spin packets at the supplementary angles $+210°$, $+270°$, and $+330°$. The generator spin packet bivector at $|v_6\rangle$ is physically antiparallel to an emission spin packet bivector at $|v_3\rangle$. Effectively, $|v_6\rangle$ contributes a zero angle projection ($k=0$) to the emission ensemble at $|v_3\rangle$. Similarly, the $|v_6\rangle$ contribution to the emission ensemble at $|v_2\rangle$ is treated as a 60° projection ($k=1$).

More generally, the projection angle from the basis vector of the generator packet to a particular basis vector of the emission ensemble is computed from the supplementary angle of the generator packet basis vector. As a result, particle projections [Fig. 8(a)] are computed in close analogy to photon projections (Fig. 4). (In the latter case, transformation to a supplementary angle basis vector in computing projections was not essential with regard to the calculational formalism because of the bidirectionality of the planar wave packets but would, nevertheless, have been appropriate from the physical perspective of the π phase differential between γ_G and γ_E.)

Then, projecting the p_G generator spin packets through $k\delta$, $k=3$, 2, and 1 in Hilbert space, yields subspace projections of the emission particle ensemble state vector $|\psi_1\rangle$, $|\psi_2\rangle$, and $|\psi_3\rangle$, respectively, where $|\psi_1\rangle$ is constructed from the single 120° projection of the generator packet at $|v_6\rangle$ to $|v_1\rangle$. Similarly, $|\psi_2\rangle$ is the 60° projection of the generator packets at $|v_5\rangle$ and $|v_6\rangle$ to $|v_1\rangle$ and $|v_2\rangle$, respectively, and $|\psi_3\rangle$ is the 0° projection of the generator packet at $|v_4\rangle$, $|v_5\rangle$, and $|v_6\rangle$ to $|v_1\rangle$, $|v_2\rangle$, and $|v_3\rangle$, respectively. These projections give

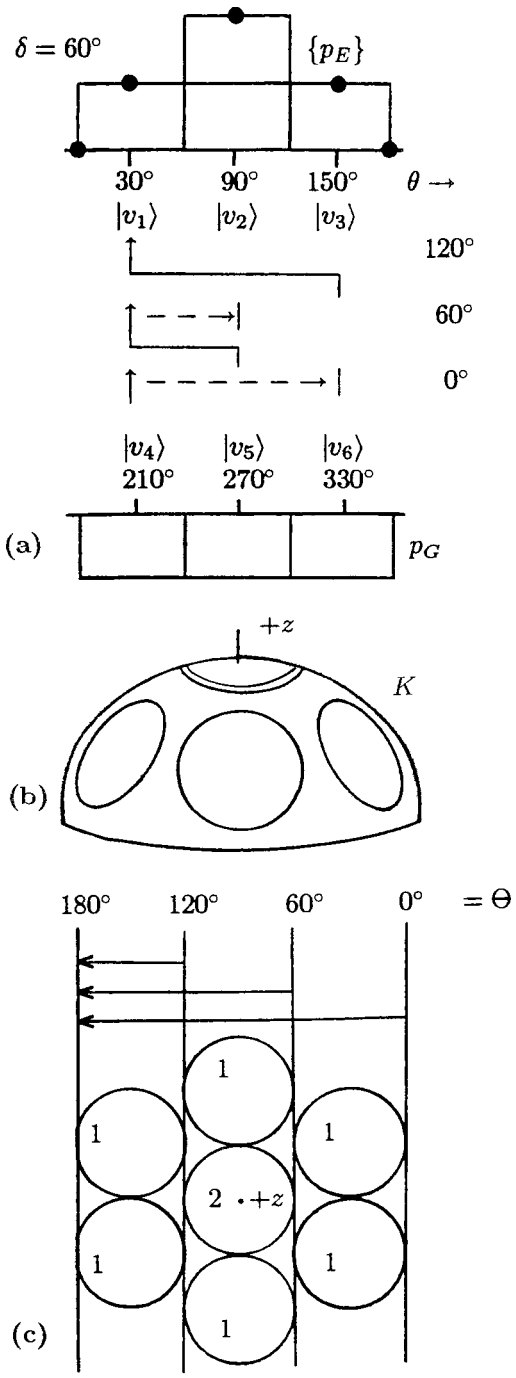

FIG. 8. Correlated particle example for $\delta=60°$ of (a) ensemble spin wave packet projection computation in an azimuthal plane, (b) schematic three-dimensional representation of ensemble spin wave packets with six singly occupied circumferential sites and one doubly occupied polar site, and (c) joint transmission probability calculation giving 8/8, 6/8, 2/8, and 0/8 when analyzers are relatively rotated by 0°, 60°, 120°, and 180°, respectively.

$$|\psi_1\rangle=c_1|v_1\rangle, \tag{55}$$

$$|\psi_2\rangle=c_1|v_1\rangle+c_2|v_2\rangle, \tag{56}$$

and

$$|\psi_3\rangle = c_1|v_1\rangle + c_2|v_2\rangle + c_3|v_3\rangle. \tag{57}$$

The norms of these projections are

$$\|\psi_k\| = \langle\psi_k|\psi_k\rangle^{1/2} = \cos\left(\frac{k\delta}{2}\right) \tag{58}$$

as in analyzer emission, but the $|\psi_k\rangle$ are now constructed over the extended generator states of p_G. Imposing Eq. (58) on Eqs. (55)–(57) we have

$$\|\psi_1\| = [c_1^2]^{1/2} = \cos\left(\frac{120°}{2}\right) = \frac{1}{2}, \tag{59}$$

$$\|\psi_2\| = [c_1^2 + c_2^2]^{1/2} = \cos\left(\frac{60°}{2}\right) = \frac{\sqrt{3}}{2}, \tag{60}$$

and

$$\|\psi_3\| = [c_1^2 + c_2^2 + c_3^2]^{1/2} = \cos\left(\frac{0°}{2}\right) = 1, \tag{61}$$

which yield the $|\psi_1\rangle$, $|\psi_2\rangle$, and $|\psi_3\rangle$ coefficients,

$$c_1 = c_3 = \frac{1}{2}, \quad c_2 = \frac{1}{\sqrt{2}}. \tag{62}$$

Since $|\psi_3\rangle$ is a projection into a subspace spanning a full complement set of basis vectors, it is equivalent to the *correlated particle superposition state*

$$|\psi_E\rangle = |\psi_3\rangle = \frac{1}{2}|v_1\rangle + \frac{1}{\sqrt{2}}|v_2\rangle + \frac{1}{2}|v_3\rangle \tag{63}$$

for the ensemble.

The squared amplitudes,

$$\langle v_1|\psi\rangle^2 = \langle v_3|\psi\rangle^2 = \frac{1}{4}, \quad \langle v_2|\psi\rangle^2 = \frac{1}{2} \tag{64}$$

specify the relative ensemble spin packet probabilities in an azimuthal plane as shown in Fig. 8(a). An inspection of this coarse $\delta = 60°$ example demonstrates that the spin packet probability is functionally consistent with $\sin\theta$ at the indicated points following normalization. From related results for photons, we can readily verify that in the limit as $\delta \to 0$ the normalized set of c_i^2 values, $i = 1$ to N/δ, is vanishingly close to $\sin\theta$.

Although we readily obtain $\cos^2(k\delta/2)$ packet expectations of 1, $\frac{3}{4}$, $\frac{1}{4}$, and 0 with $k\delta/2 = 0°$, 30°, 60°, and 90°, respectively, we must remember that Eq. (64) and Fig. 8(a) represent packet probabilities in an arbitrary azimuthal plane. However, zero angular momentum of every correlated pair p_G, p_E imposes rotational symmetry upon the full distribution of packets. Accordingly, Fig. 8(a) is also the distribution of spin packets in an arbitrary azimuthal plane and we can immediately construct a full three-dimensional distribution of ensemble spin packets mapped onto a 2π hemispherical surface as shown in Fig. 8(b).

At $+z$ in K, the central (pole) packet site is doubly occupied while the remaining six circumferential sites are singly occupied. Symmetry with p_G further facilitates identification of the two ensemble members. One member consists of the full complement set of seven spin packets while the other member is the single additional spin packet at the $+z$ pole. Clearly, the circumferential distribution of six sites is not an exact rotational symmetry about $+z$ and the mapping itself is not accomplished without some minor areal distortion of the a_δ. However, both of these concerns are attributable to the finiteness of the present $\delta = 60°$ example and are resolved as $\delta \to 0$. The associated generator particle p_G is represented by a full complement seven-site 2π hemispherical zone oriented at $-z$ in K.

We want to use this three-dimensional distribution to compute joint transmission probabilities when a correlated particle source is positioned between opposed Stern-Gerlach analyzers A_1 and A_2. The respective magnetic field vectors $\mathbf{B}_1$ and $\mathbf{B}_2$ of the analyzers are rotated by Θ relative to each other, but these vectors are otherwise random in K. We choose spin up as the open channel of A_1 and spin down as the open channel of A_2. In the present representation, the probability for joint analyzer transmission is then equivalently the two-vector probability of intersecting a member in the $\{p_E\}$ distribution with $\mathbf{B}_1$ and intersecting the full complement p_G with $-\mathbf{B}_2$. This determination can be greatly simplified by symmetry properties. Since $\{p_E\}$ is rotationally symmetric, we can azimuthally rotate the pole of p_G by $\Theta + \pi$ at any φ and observe that the joint intersection of a single vector with $\{p_E\}$ members and a rotated p_G is equivalent to the above two-vector probability problem [see Fig. 9].

The single vector joint intersection is readily evaluated in the present $\delta = 60°$ example. When p_G is rotated by $\Theta + \pi$ about $\{p_E\}$ where $\Theta = k\delta = 0°$, 60°, 120°, or 180°, the joint overlap of p_G with $\{p_E\}$ is calculated in each case from the transection of the $\{p_E\}$ spin packets by a plane. That plane is identified as the base of the p_G hemispherical zone. The $\{p_E\}$ transections for these Θ are depicted in Fig. 8(c).

For $\Theta = 0°$, the joint overlap is all eight spin packets and the joint transmission probability is

$$P_p(0°) = \frac{1}{28}(8), \tag{65}$$

where the normalization factor 28 accounts for all of the spin packet sites that must be interrogated by the single vector. Since there are two ensemble members, $\{p_E\}$ represents 2×7 sites. However, there are an additional 2×7 sites that must be included representing the 50% chance of the single vector not intersecting $\{p_E\}$. Similarly, we have

$$P_p(60°) = \frac{1}{28}(6), \quad P_p(120°) = \frac{1}{28}(2),$$

$$P_p(180°) = \frac{1}{28}(0). \tag{66}$$

These probabilities can be summarized and reorganized as

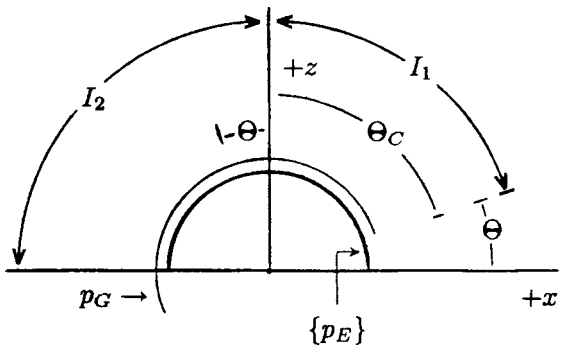

FIG. 9. Calculational technique for determining correlated particle joint transmission probability by rotating p_G zone through $\Theta + \pi$ in K.

$$P_p(k\delta) = \frac{8}{28} \sum_{i=1}^{3-k} \langle v_i | \psi \rangle^2 = \frac{1}{2}\left(\frac{4}{7}\right) \sum_{i=1}^{3-k} c_i^2 = \frac{1}{2}\left(\frac{4}{7}\right) \cos^2\left(\frac{k\delta}{2}\right). \tag{67}$$

The origin of the extracted $\frac{1}{2}$ factor in Eq. (67) may be identified as the probability of intersecting the 2π solid angle of p_G at some random orientation (e.g., that of the axis for a Stern-Gerlach channel). The adjacent factor is the fractional occupancy of spin packets in $\{p_E\}$ designated as F_p. Since the probability of encountering a spin packet on $\{p_E\}$ is unity at the polar site and $\frac{1}{2}$ for the six circumferential sites, we have $F_p = \frac{1}{7}(1 + \frac{1}{2} \times 6) = \frac{4}{7}$. The summation factor is recognized as equivalent in form to the corresponding summation factor in Eq. (35) for photons but here, for $\delta = 60°$, yields $\cos^2(k\delta/2)$. This similarity originates with the construction of $\{p_E\}$ states from projections in azimuthal planes in analogy to the construction of $\{\gamma_E\}$ states from projections in the plane orthogonal to the propagation axis. Then, despite the three-dimensionality of $\{p_E\}$, probabilities in azimuthal planes are functionally analogous to the probabilities associated with $\{\gamma_E\}$. The functional analogs of these probabilities are related by a $\theta \rightarrow \theta/2$ change of variable. This is exemplified by the Fig. 8(a) $\{p_E\}$ probabilities which can be fitted to a $\sin\theta$ function. We recall that the Fig. 4 $\{\gamma_E\}$ probabilities can be fitted to $\sin(2\theta)$.

The functional aspect of $P_p(k\delta)$ that is uniquely related to the three-dimensionality of spin packet structure resides in F_p.

Upon proceeding toward the limit $\delta \rightarrow 0$, we have

$$P_p(k\delta) = \frac{1}{2} F_p \sum_{i=1}^{N-k} \langle v_i | \psi_E \rangle^2 = \frac{1}{2} F_p \cos^2\left(\frac{k\delta}{2}\right) \tag{68}$$

for arbitrarily large $2N = 2\pi/\delta$ in a $2N$-dimensional Hilbert space where N basis vectors span a full complement spin structure zone. Recognizing that the (exact) value of the spin packet occupation fraction arises from the full three-dimensional distribution of spin packets, we have left that value unspecified for the moment as F_p.

When we reach the limit $\delta \rightarrow 0$, the corresponding Hilbert space is infinite dimensional and the integral form of Eq. (68) in analogy to Eq. (38) is

$$P_p(\Theta) = \frac{1}{2} F_p \int_0^{\pi - \Theta} E_p(\theta)\, d\theta = \frac{1}{2} F_p \cos^2\left(\frac{\Theta}{2}\right), \tag{69}$$

where $E_p(\theta)$ represents the spin packet probability. The solution to Eq. (69) is $E_p(\theta) = \sin\theta$ and gives the functional form of the Fig. 3 $\{p_E\}$ probability envelope.

We are reminded that projections for $\{p_E\}$ were computed in an arbitrary azimuthal plane which was selected as xz. In these projections, θ was treated as the polar angle referenced to $+x$ in K. This choice was convenient in computing the $\sin\theta$ $\{p_E\}$ probability envelope. However, since θ is merely an integration variable, we are free to rotationally translate $\theta = 0$ by $\pi/2$ to $+z$. In an azimuthal plane we can treat θ as a polar coordinate about $+z$ and spin packet probabilities are then functionally given by $E_p(\theta) = \cos\theta$. This $\cos\theta$ spin packet probability is applicable to an arbitrary azimuthal plane, but because of zero angular momentum for all correlated pairs, we have rotational symmetry about $+z$ which requires that $\cos\theta$ is equivalently also the spin packet distribution in any azimuthal plane. (This equivalence of spin packet probability and distribution in azimuthal planes was not applicable in particle analyzer emission.)

The construction of the members of the correlated particle emission ensemble $\{p_E\}$ is then trivially obtained from the spin packet distribution in an azimuthal plane, unlike that of the analyzer emission ensemble $\{p_e\}$. Zero net angular momentum for all p_G, p_E correlated pairs requires rotational symmetry about the p_G orientation. This symmetry together with the spin packet contiguity identifies the Fig. 3 spin packet expectation rows as the ensemble members of $\{p_E\}$ with each row representing the member's spin packet distribution in any arbitrary azimuthal plane. The three-dimensional distribution of the ensemble members consists of coaxial zones about $+z$ in K with respective planar arc spans Δ_p given by the Fig. 3 rows. The frequency distribution or *density* of ensemble members is given by $\cos\theta$ as a function of θ ($\leqslant \pi/2$). The $\{p_E\}$ members, with a continuous spectrum of Δ_p values ranging from 0 to π, have an average ensemble member planar arc span $\langle \Delta_p \rangle = 2$.

In the particle frame K, all $\{p_E\}$ members and p_G are oriented at $+z$ and $-z$, respectively, as shown schematically in Fig. 10. In the laboratory frame, the orientations of p_G and p_E for each correlated pair are mutually antiparallel but are otherwise random.

As we seek the joint transmission probability, we must proceed with care. Equation (69) is explicitly constructed in an azimuthal plane of K. This restriction is perfectly acceptable with regard to ascertaining the azimuthal plane distribution of ensemble members (and the spin packets) since that distribution is necessarily rotationally symmetric for zero net angular momentum. However, treating Eq. (69) as a joint transmission result effectively assumes that the opposed Stern-Gerlach analyzers have their $\mathbf{B}_1$ and $\mathbf{B}_2$ axes (rotationally separated by some Θ) in the same azimuthal plane in K. This assumption is not generally valid since the $\mathbf{B}_1, \mathbf{B}_2$ pair (aside from a fixed relative Θ rotation) has totally random orientation in K. Accordingly, we must rigorously compute the joint analyzer transmission probability $P_p(\Theta)$ for appro-

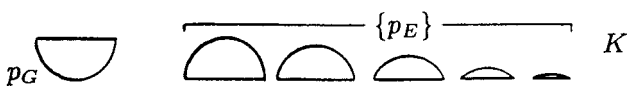

FIG. 10. Correlated particles in particle frame K showing representative ensemble members of $\{p_E\}$ with a $\cos\theta$ distribution of Δ_p arc spans and antiparallel mate p_G.

priately randomized orientations of the $\mathbf{B}_1,\mathbf{B}_2$ pair.

We again use the calculational methodology of rotating p_G by $\Theta+\pi$ with respect to $\{p_E\}$ in order to reduce the joint transmission problem to that of a single vector intersection. Figure 9 is still applicable.

Without loss of generality, we can select an orientation of p_G in the xz plane at some arbitrary Θ and at $\varphi=\pi$ in the correlated particle frame K. The base of the p_G hemispherical zone is the plane defined by

$$\tan\Theta_C=\frac{x}{z}=\frac{\sin\theta\cos\varphi}{\cos\theta}, \tag{70}$$

where θ is the azimuthal integration variable in the particle frame and Θ_C is the complement of Θ. Then θ, functionally dependent upon φ, is

$$\theta(\varphi)=\tan^{-1}\left(\frac{\tan\Theta_C}{\cos\varphi}\right). \tag{71}$$

The transmission probability is determined by computing the three-dimensional angular surface integral I_1 over the ensemble spin packet distribution in $x<0$ and also the corresponding integral I_2 over the ensemble spin packet distribution in $x>0$, but bounded by the p_G base (Fig. 9). Symmetry permits φ integration over a quadrant for both integrals and doubling their values. The quantity $\cos\theta$ in these integrals is effectively the density function of spin packets as determined above and expressed azimuthally.

The normalization factor of 2π is simply the angular integral over the hemisphere. A factor of $\frac{1}{2}$ must also be included to account for the p_G transmission probability. Then the joint analyzer transmission probability is

$$\begin{aligned}P_p(\Theta)&=\frac{1}{2}\,\frac{2I_1+2I_2}{2\pi}\\&=\frac{1}{2\pi}\int_0^{\pi}\cos\theta\sin\theta\,d\theta\int_{\pi/2}^{\pi}d\varphi\\&\quad+\frac{1}{2\pi}\int_0^{\pi/2}\int_0^{\theta(\varphi)}\cos\theta\sin\theta\,d\theta d\varphi\\&=\frac{1}{8}+\frac{1}{4\pi}\int_0^{\pi/2}\sin^2\left[\tan^{-1}\left(\frac{\tan\Theta_C}{\cos\varphi}\right)\right]d\varphi\\&=\frac{1}{4}\sin^2\frac{\Theta_C}{2}=\frac{1}{4}\cos^2\frac{\Theta}{2}.\end{aligned} \tag{72}$$

The spin packet occupancy fraction in the $\delta\to 0$ limit is

$$F_p=\frac{4I_1}{2\pi}=\frac{1}{2}, \tag{73}$$

which is a decrease from the $\frac{4}{7}$ approximation associated with the coarse $\delta=60°$ example. From Eq. (69), we recognize that F_p is a $\frac{1}{2}$ factor extracted from the $\frac{1}{4}$ numerical coefficient in Eq. (72).

The calculation of the predicted joint probability for correlated particles proceeds in a manner analogous to that of photons. However, for the three-dimensional spin packet structure, the detection interaction cross section over $\{p_E\}$ is proportionate to the average area of the ensemble zones. Accordingly, the relevant parameter is F_p and not $\langle\Delta_p\rangle$. With the cross section linear to the zone area, the average detection efficiency over $\{p_E\}$ is

$$\langle\eta_E\rangle=F_p\eta=\frac{1}{2}\eta, \tag{74}$$

where η is the detection efficiency for a full complement particle. Equation (74) constitutes the *linearity* criterion for particle detectors. Equation (74) is dependent only upon the angular geometrical aspects of the spin structure zones and is not a function of the amplitude coefficient b_p.

Then, with the quantities $R(\Theta)$, R_0, R_T, and f defined in direct analogy to those of correlated photons, the ''joint probability'' for particles is

$$\wp_p(\Theta)=\frac{R(\Theta)}{R_0}=\frac{R_T f P_p(\Theta)\eta^2}{R_T f\eta\langle\eta_E\rangle}=\frac{1}{2}\cos^2\frac{\Theta}{2}, \tag{75}$$

in agreement with the probabilistic interpretation of quantum mechanics.

A comparison to correlated photons readily demonstrates that this agreement is a consequence of natural enhancement, and when $\langle\eta_E\rangle>\frac{1}{2}\eta$ the locally real representation is testable with respect to the probabilistic interpretation.

IV. DISCUSSION

The inherent asymmetry of the correlated locally real states for both photons and particles, as manifested by the packet occupation fraction, has important implications with regard to Bell's theorem [4]. It has been shown that ''nonenhancement'' is an implicit assumption of Bell's theorem [25]. This assumption is generally regarded as plausible since it requires that insertion of an analyzer in the path of a correlated photon or particle must reduce or, at least, leave invariant the resultant detection probability. Conversely, Bell's theorem is not applicable to the class of hidden variable theories exhibiting enhancement, i.e., detection probability potentially increases upon inserting an analyzer. Accordingly, this class has not been excluded by performed experiments. However, theories exhibiting enhancement are not generally perceived as a viable alternative to the probabilistic interpretation because of the apparent implausibility of enhancement and its typically arbitrary imposition in those theories. It is therefore a critical aspect of the present locally real represen-

tation that enhancement arises as a natural and plausible property.

In retrospect, is of some interest here to note the compelling and prognostic advice of Ferrero, Marshall, and Santos [19] that it would be productive to examine modifications of the standard quantum mechanical formalism in the interests of achieving compatibility with local realism despite the successes of the probabilistic interpretation of quantum mechanics. They anticipated that these modifications would yield a theory that naturally violated Bell's plausible assumptions [4,25].

Similarly, it is of further interest here that several investigations, including those of Selleri and Zeilinger [20], Lepore and Selleri [21], and Ferrero, Marshall, and Santos [19], have identified the detector low efficiency ''loophole'' as a likely critical aspect of a viable locally real representation.

In the present context, the testable consequences for which the locally real representation derived here diverges from quantum mechanics relate to the use of a detector that exceeds the linearity criterion. Nevertheless, the divergence is subtle in that the numerical coefficients of the joint detection probabilities Eqs. (45) and (75) are altered, but the cosine squared function of Θ does not change. In contrast, a more readily discernible linearization of Θ dependence is predicted for those locally real hidden variable theories consistent with Bell's inherent assumptions [4,25].

It is also pertinent here to examine the relative divergence of the locally real representation from the quantum mechanical treatment of spatially separated superposition states. These states arise when considering phenomena involving devices such as beam splitters and two-channel analyzers.

Quantum mechanically, the probabilistic photons and particles are divided by such devices into two states that are necessarily represented as a nonlocal spatially separated superposition state. Conversely, in the locally real representation, the outputs of these devices produce two independent wave structures. Objectively, one structure is excitation bearing and the other is empty.

When only ''non-analyzer'' devices such as simple beam splitters are involved, the independent wave structures from both output channels are each immediately compatible with representation by the wave functions of the quantum mechanical formalism, e.g., $\Phi(z,t)$ or $\Psi(x,t)$, but not with the probabilistic interpretation of that formalism. However, when the devices include two-channel analyzers, the complete objective specifications of the two independent output wave functions must now be constructed from analyzer emission states. Each output wave function can then objectively be identified as a particular ensemble member derived from those analyzer emission states.

Consequently, quantum mechanical spatially separated superposition states associated with ''nonanalyzer'' as well as analyzer two-channel phenomena can both be given a locally real representation. (This would include phenomena that are supposedly characteristic of purely quantum mechanical behavior such as ''interaction-free measurement'' [29,30].) We reiterate, though, that analyzer phenomena necessitate an ensemble construction augmenting the wave functions $\Phi(z,t)$ and $\Psi(x,t)$ of the quantum mechanical formalism.

The necessary imposition of an ensemble construction on the wave functions of the quantum mechanical formalism was, of course, initially seen in the context of single propagating entities when analyzer measurements were considered.

Clearly then, there is some profound physical interaction that underlies the significant divergence of the locally real representation from the quantum mechanical formalism when analyzer measurement is considered. To understand this divergence, we first consider a set of individual (nonanalyzer) detector measurements performed on a large number of discrete photons or particles each of which is prepared under identical experimental conditions. (The appropriate wave function might represent a superposition of energy states.) Individual measurements reveal a random state instantaneously occupied by the excitation at the time of measurement. Accordingly, the collective measurements then objectively yield the constituent states in their proper statistical distribution.

However, from the locally real perspective, analyzer measurements are distinctive in that they are noninstantaneous processes that occur as a wave structure is incident on an analyzer. The excitation, migrating on the diminishing constituent packets entering the analyzer, locks into the δ-form superpacket forming along the analyzer's axis if that axis should happen to intersect one of those constituent packets. Effectively, the analyzer inherently biases the excitation locus to the analyzer's axis for these events. Subjectively, then, we lose information regarding the excitation's instantaneous locus as the incident packets begin to enter the analyzer.

Accordingly, we postulate that analyzer measurements are noninstantaneous processes that bias the final excitation location to the particular state at the analyzer's axis. If such a process has physical validity, then the quantum mechanical treatment that places analyzer measured states on an equal footing with conventional detector measured states is in doubt. That position is taken in the present paper and provides the basis for proceeding with the derivation of the ensemble of analyzer emission states on which the excitation may instantaneously reside prior to analyzer measurement.

V. CONCLUSIONS

We must emphasize that the locally real representation presented here does not present any conflict with the calculational success of the standard quantum mechanical formalism. We have noted that we begin with the quantum mechanical formalism that specifies the wave functions for photons and particles along the propagation axis, respectively $\Phi(z,t)$ and $\Psi(x,t)$ in configuration space, and treat these wave functions as incomplete. We derive an ensemble wave function associated with a source that yields emission states. The wave functions of these emission states are naturally augmented with field variables that define outcomes for measurement processes normally requiring the invocation of a nonlocal probabilistic interpretation. However, these augmented emission state wave functions remain fully consistent with the standard quantum formalism (but not with the probabilistic interpretation) as valid solutions of the appro-

priate wave equation and boundary conditions. The completely specified wave function of an emitted photon or particle objectively determines transmission through a subsequent analyzer. The resultant locally real representation gives exact agreement with quantum mechanics for photon transmission through successive polarization analyzers, for particle transmission through successive Stern-Gerlach analyzers, for correlated pairs of photons, and for correlated pairs of particles while providing testable consequences. Spatially separated quantum mechanical superposition states can also be given a locally real representation.

The construction of the respective ensembles associated with these phenomena proceeds in a self-consistent manner. An ensemble of states (for photons or for particles) described by a wave function (ϕ or ψ) is formed from projections in an infinite dimensional Hilbert space at the emission source for $t<0$. The states are specifications of (planar or spin) wave packets. At $t=0$, a random member formed from the states of the ensemble is emitted as a stochastic process with specific objectively real field variable values of packet arc span (Δ_γ or Δ_p) and orientation (θ_γ or θ_p,φ_p). The wave function is scaled by an amplitude coefficient (b_γ or b_p). The general wave function of the emitted member for $t\geqq 0$ can be expressed in configuration space [$\Phi(z,t;\Delta_\gamma,\theta_\gamma,b_\gamma)$ or $\Psi(x,t;\Delta_p,\theta_p,\varphi_p,b_p)$] along the propagation axis (z or x). Effectively, the transition from the ensemble state to a particular emission state ($\phi\rightarrow\Phi$ or $\psi\rightarrow\Psi$) can be defined as ''stochastic realism'' [19].

For any similarly generated emitted members of the ensemble, regardless of the fixed field variable values, the associated wave function structures (Φ or Ψ) are all essentially identical when examined only with respect to the configuration and momentum space variables along the propagation axis. A measurement procedure based on these variables for a particular emitted member may be used to reveal a single point on the envelope of the wave function's squared modulus ($\Phi^*\Phi$ or $\Psi^*\Psi$). That point is determined by the value that the migrating excitation happens to assume at the instant of measurement on the structure of the wave function. When applied to many similarly generated events, such measurements map the entire envelope of the wave function's squared modulus along the propagation axis.

More significantly in the present context, for a particular discrete entity (photon or particle), with field variable values then necessarily objectively fixed, the transmission outcome through an analyzer (polarization or Stern-Gerlach) is fully determined for all $t>0$ and can be identified as ''deterministic realism'' [19]. Quantum mechanically, the transmission outcomes are interpreted as evidence that these entities are necessarily probabilistic. The perception that photons and particles are probabilistic entities is derived from the biased selection of a particular constituent state by the measurement analyzer.

When the wave function (Φ or Ψ) for a particular discrete entity objectively specifies fewer than a full complement of packets ($\Delta_\gamma<\pi/2$ or $\Delta_p<\pi$), transmission through an analyzer increases the arc span to a full complement and naturally enhances detectability. The correlated emission states exhibiting this property of natural enhancement are explicitly local in contrast to quantum mechanical correlated states which are necessarily nonlocally entangled. The perception of entanglement is a consequence of the subtlety of enhancement.

[1] L. de Broglie, *Electrons et Photons* (Gauthier-Villars, Paris, 1928); *The Current Interpretation of Wave Mechanics: A Critical Study* (Elsevier, Amsterdam, 1969).
[2] N. Bohr, Phys. Rev. **48**, 696 (1935).
[3] A. Einstein, B. Podolsky, and N. Rosen, Phys. Rev. **47**, 777 (1935).
[4] J. S. Bell, Physics (Long Island City, N.Y.) **1**, 195 (1964).
[5] J. F. Clauser and A. Shimony, Rep. Prog. Phys. **41**, 1881 (1978), and references therein; A. Aspect, J. Dalibard, and G. Roger, Phys. Rev. Lett. **49**, 1804 (1982).
[6] K. R. Popper, *Quantum Theory and the Schism in Physics* (Rowman and Littlefield, Totowa, NJ, 1982).
[7] M. Zukowski, D. Kaszlikowski, and E. Santos, Phys. Rev. A **60**, R2614 (1999).
[8] N. Gisin and B. Gisin, Phys. Lett. A **260**, 323 (1999).
[9] R. Foadi and F. Selleri, Phys. Rev. A **61**, 012106 (2000).
[10] J.-A. Larsson, Phys. Rev. A **57**, 3304 (1998); Phys. Lett. A **256**, 245 (1999).
[11] A. Casado, T. W. Marshall, and E. Santos, J. Opt. Soc. Am. B **15**, 1572 (1998).
[12] M. Ferrero and E. Santos, Found. Phys. **27**, 765 (1997).
[13] S. F. Huelga, T. W. Marshall, and E. Santos, Europhys. Lett. **38**, 249 (1997).
[14] S. F. Huelga, T. W. Marshall, and E. Santos, Phys. Rev. A **54**, 1798 (1996).
[15] E. Santos, Phys. Lett. A **212**, 10 (1996).
[16] S. F. Huelga, M. Ferrero, and E. Santos, Phys. Rev. A **51**, 5008 (1995).
[17] J. Barretto Bastos Filho and F. Selleri, Found. Phys. **25**, 701 (1995).
[18] T. W. Marshall and E. Santos, Phys. Rev. A **39**, 6271 (1989).
[19] M. Ferrero, T. W. Marshall, and E. Santos, Am. J. Phys. **58**, 683 (1990).
[20] F. Selleri and A. Zeilinger, Found. Phys. **18**, 1141 (1988).
[21] V. L. Lepore and F. Selleri, Found. Phys. **3**, 203 (1990).
[22] E. Santos, Phys. Rev. Lett. **66**, 1388 (1991).
[23] M. Ferrero and E. Santos, Phys. Lett. A **116**, 356 (1986).
[24] S. Mirell, Phys. Rev. A **50**, 839 (1994).
[25] J. F. Clauser and M. A. Horne, Phys. Rev. D **10**, 526 (1974).
[26] D. Bohm, Phys. Rev. **85**, 166 (1952).
[27] M. Rabinowitz, Mod. Phys. Lett. B **9**, 763 (1995).
[28] S. Mirell and D. Mirell, e-print quant-ph/9911076.
[29] A. C. Elitzur and L. Vaidman, Found. Phys. **23**, 987 (1993).
[30] P. G. Kiwat, H. Weinfurter, T. Herzog, and A. Zeilinger, Phys. Rev. Lett. **74**, 4763 (1995).